Bi-directional signaling by Semaphorin 1a during central synapse formation in Drosophila. Nat. Neurosci. **5**, 1294–1301.

51) Kuhn, T.B., Brown, M.D., Wilcox, C.L., Raper, J.A. and Bamburg, J.R. (1999) Myelin and collapsin-1 induce motor neuron growth cone collapse through different pathways: inhibition of collapse by opposing mutants of rac1. J. Neurosci. **19**, 1965–1975.

52) Zanata, S.M., Hovatta, I., Rohm, B. and Puschel, A.W. (2002) Antagonistic effects of Rnd1 and RhoD GTPases regulate receptor activity in Semaphorin 3A-induced cytoskeletal collapse. J. Neurosci. **22**, 471–477.

53) Di Paolo, G., Pellegrini, L., Letinic, K., Cestra, G., Zoncu, R., Voronov, S. *et al.* (2002) Recruitment and regulation of phosphatidylinositol phosphate kinase type 1γ by the FERM domain of talin. Nature **420**, 85–89.

54) Ling, K., Doughman, R.L., Firestone, A.J., Bunce, M.W. and Anderson, R.A. (2002) Type Iγ phosphatidylinositol phosphate kinase targets and regulates focal adhesions. Nature **420**, 89–93.

(Received Mar. 29, 2010; accepted Apr. 8, 2010)

nature immunology

Semaphorins guide the entry of dendritic cells into the lymphatics by activating myosin II

Hyota Takamatsu[1,2], Noriko Takegahara[1,2], Yukinobu Nakagawa[1,2,3], Michio Tomura[4], Masahiko Taniguchi[5], Roland H Friedel[6], Helen Rayburn[7], Marc Tessier-Lavigne[8], Yutaka Yoshida[9], Tatsusada Okuno[1,2], Masayuki Mizui[2,10], Sujin Kang[1,2], Satoshi Nojima[1,2,11], Tohru Tsujimura[12], Yuji Nakatsuji[13], Ichiro Katayama[3], Toshihiko Toyofuku[1,2], Hitoshi Kikutani[2,10] & Atsushi Kumanogoh[1,2]

The recirculation of leukocytes is essential for proper immune responses. However, the molecular mechanisms that regulate the entry of leukocytes into the lymphatics remain unclear. Here we show that plexin-A1, a principal receptor component for class III and class VI semaphorins, was crucially involved in the entry of dendritic cells (DCs) into the lymphatics. Additionally, we show that the semaphorin Sema3A, but not Sema6C or Sema6D, was required for DC transmigration and that Sema3A produced by the lymphatics promoted actomyosin contraction at the trailing edge of migrating DCs. Our findings not only demonstrate that semaphorin signals are involved in DC trafficking but also identify a previously unknown mechanism that induces actomyosin contraction as these cells pass through narrow gaps.

Dendritic cells (DCs) are highly mobile antigen-presenting cells that use a coordinated trafficking system to ensure that they are present in the right place and at the right time to induce proper immune responses[1]. Before encountering foreign antigens, DCs reside as sentinels in the peripheral tissues. However, after antigen exposure, DCs migrate from the peripheral tissues to lymphoid organs, where they activate T cells. To exit the periphery, DCs must migrate toward and enter the initial lymphatics[2,3]. This is an active process that involves chemokines and adhesion molecules[4–8]. Transmission electron microscopy has shown that DCs must undergo considerable morphological changes to pass through endothelial junctions[9,10]. Non-muscle myosin II is needed to propel DC cellular bodies forward and enable them to pass through narrow gaps[11]. However, it is still unknown how DCs interact with the lymphatic endothelium during transmigration and whether the lymphatics, in turn, control and affect DC mobilization to coordinate their cytoskeletal dynamics, including contraction and adhesion disassembly.

Semaphorins were initially identified as axonal guidance cues that determine the direction and migration of neurons during neurogenesis[12]. In addition, they have diverse and important functions in other physiological processes, including heart development[13], vascular growth[14], tumor progression[15,16] and immune responses[17]. Several semaphorins have costimulatory molecule–like activities that promote the activation of B cells[18], T cells[19], DCs[20] and macrophages[21] through cell-cell interactions. In the nervous system, semaphorins regulate cell motility and morphology through interaction with receptors of the plexin family[22]. A similar role for semaphorins in regulating the migration of cells of the immune response has been proposed. Among the plexin family members, plexin-A1 represents the main receptor for class III and class VI semaphorins. Together with ligand-binding neuropilins, plexin-A1 transduces repulsive axon-guidance signals for soluble class III semaphorins[23]. Independently of neuropilins, plexin-A1 functions in neurogenesis and cardiogenesis as a receptor for the class VI transmembrane semaphorins Sema6C and Sema6D[13,24]. In the immune system, plexin-A1 is expressed specifically in DCs, and it may facilitate DC-mediated stimulation of T cells[25]. Plexin-A1–deficient (*Plxna1*$^{-/-}$) mice have severe defects in antigen-specific T cell responses[20]. However, it is still unclear whether semaphorins physiologically regulate the migration of cells of the immune response via plexin receptors.

Here we demonstrate that plexin-A1 has a crucial role in DC trafficking, particularly during entry into lymphatics. Specifically, we show that Sema3A produced in the lymphatics functioned as a ligand for the plexin-A1–neuropilin 1 (NRP1) receptor complex expressed by DCs. Furthermore, we demonstrate that Sema3A acted on the rear side of DCs, where plexin-A1 is localized. Sema3A induced

[1]Department of Immunopathology, Research Institute for Microbial Diseases, Osaka University, Suita, Japan. [2]World Premier International Immunology Frontier Research Center, Osaka University, Suita, Japan. [3]Department of Dermatology, Osaka University Graduate School of Medicine, Suita, Japan. [4]Laboratory for Cell Function and Dynamics, Advanced Technology Development Center, Brain Science Institute, RIKEN, Wako, Japan. [5]Department of Biochemistry, Cancer Research Institute, Sapporo Medical University School of Medicine, Sapporo, Japan. [6]Institute of Developmental Genetics, Helmholtz Center Munich, Neuherberg, Germany. [7]Department of Developmental Biology, Stanford University, Stanford, California, USA. [8]Division of Research, Genentech, South San Francisco, California, USA. [9]Division of Developmental Biology, Cincinnati Children's Hospital Medical Center, Cincinnati, Ohio, USA. [10]Department of Molecular Immunology, Research Institute for Microbial Diseases, Osaka University, Suita, Japan. [11]Department of Pathology, Osaka University Graduate School of Medicine, Suita, Japan. [12]Department of Pathology, Hyogo College of Medicine, Nishinomiya, Japan. [13]Department of Neurology, Osaka University Graduate School of Medicine, Suita, Japan. Correspondence should be addressed to A.K. (kumanogo@ragtime.biken.osaka-u.ac.jp).

Received 23 February; accepted 10 May; published online 30 May 2010; doi:10.1038/ni.1885

phosphorylation of the myosin light chain (MLC) to promote actomyosin contraction, which resulted in more DC transmigration as these cells passed through narrow gaps.

RESULTS

Impaired DC trafficking to draining lymph nodes in *Plxna1*$^{-/-}$ mice

Antigen-specific T cell generation is severely impaired in *Plxna1*$^{-/-}$ mice[20]. However, it is unclear how plexin-A1 is involved in antigen-specific T cell priming. To investigate these mechanisms in greater detail, we activated OT-II T cells (with an ovalbumin (OVA)-specific T cell antigen receptor)[26] in wild-type and *Plxna1*$^{-/-}$ mice. OT-II T cells labeled with the cytosolic dye CFSE proliferated extensively after subcutaneous administration of OVA peptides in complete Freund's adjuvant to wild-type recipient mice (**Fig. 1a**). In contrast, antigen-specific proliferative responses were much lower when we transferred OT-II T cells into *Plxna1*$^{-/-}$ recipient mice (**Fig. 1a**), which confirmed the importance of plexin-A1 in antigen-specific T cell responses (**Supplementary Fig. 1a**).

Antigen-specific T cells are primed in the draining lymph nodes via encounters with antigen-pulsed DCs[27]. To examine the effect of *Plxna1*$^{-/-}$ DCs on DC–T cell interactions in the draining lymph nodes, we obtained OVA-pulsed DCs from wild-type or *Plxna1*$^{-/-}$ mice, labeled them with the cell-tracking dye CMTMR (5-(and-6)-(((4-chloromethyl)benzoyl) amino)tetramethylrhodamine), injected them into the footpads of wild-type recipient mice and analyzed the popliteal lymph nodes by two-photon microscopy. When we injected wild-type DCs into the footpads, CMTMR-labeled DCs were abundantly distributed and localized throughout the T cell area of the draining lymph nodes (**Fig. 1b**). In contrast, when we injected *Plxna1*$^{-/-}$ DCs, we found only minimal DCs in the draining lymph nodes of recipient mice (**Fig. 1b**), which indicated that *Plxna1*$^{-/-}$ DCs had impaired migratory abilities. To quantitatively compare the *in vivo* migratory activities of wild-type and *Plxna1*$^{-/-}$ DCs, we injected CFSE-labeled DCs into the footpads of wild-type mice and examined their arrival in the draining lymph nodes. *Plxna1*$^{-/-}$ DCs showed impaired migratory activity compared with that of wild-type DCs (**Fig. 1c** and **Supplementary Fig. 1b**). We also analyzed the migration of endogenous DCs under steady-state conditions. *Plxna1*$^{-/-}$ mice had fewer CD11c^{+} major histocompatibility complex class II–high and CD11c^{+}CD4^{-}CD8^{-} migratory DC subsets in the skin-draining lymph nodes[6,28] (**Supplementary Fig. 1c**). Because the expression of plexin-A1 increased during DC maturation (**Supplementary Fig. 2b**), we investigated the trafficking of endogenous DCs to the draining lymph nodes under inflammatory conditions. We applied fluorescein isothiocyanate (FITC) epicutaneously to an area of skin that drains to the brachial lymph nodes and counted FITC^{+} DCs in the draining lymph nodes[29,30]. We found considerably less accumulation of FITC^{+} DCs in brachial lymph nodes in *Plxna1*$^{-/-}$ mice than in wild-type mice (**Fig. 1d**). Collectively these findings indicate that plexin-A1 is critically involved in DC trafficking and that impaired DC migration is the main reason for defective T cell priming in *Plxna1*$^{-/-}$ mice.

Impaired transmigration of *Plxna1*$^{-/-}$ DCs

To determine which step requires plexin-A1 during DC trafficking from the peripheral tissues to the lymphatics[3], we studied antigen uptake, interstitial migration toward the lymphatics in response to chemokines and transmigration across the lymphatics in greater detail (**Supplementary Fig. 3**). We did not find differences between wild-type and *Plxna1*$^{-/-}$ DCs in their antigen uptake (**Fig. 2a**). In addition, there were no differences in the ability of DCs to migrate in response to the chemokines CCL19, CCL21 or CXCL12 in Transwell systems (**Fig. 2b**), or in their ability to sense direction in a chemokine-gradient assay (**Fig. 2c** and **Supplementary Movie 1**). Consistent with those findings, wild-type and *Plxna1*$^{-/-}$ DCs had similar expression of the chemokine receptors CCR7 and CXCR4 (**Fig. 2d**). These results indicate that plexin-A1 is not required for antigen uptake or chemokine responsiveness during migration.

To assess the role of plexin-A1 in the transmigration process *in vivo*, we adoptively transferred CFSE-labeled wild-type or *Plxna1*$^{-/-}$ DCs into the dermis of oxazolone-treated mice and assessed the fate of emigrating DCs[7]. Large numbers of *Plxna1*$^{-/-}$ DCs were retained along lymphatics positive for the lymphatic endothelial cell marker LYVE-1 in the dermis of recipient mice 24 h after adoptive transfer (**Fig. 3a**), an activity we did not observe with wild-type DCs. This indicated that *Plxna1*$^{-/-}$ DCs have impaired transmigration across the lymphatics.

By time-lapse imaging we investigated whether plexin-A1 deficiency in DCs affected the initial contacts between DCs and lymphatic endothelial cells. Wild-type DCs interacted with endothelial cells at the cell-cell junctions of lymphatic endothelial cells and transmigrated across the endothelial cells (**Fig. 3b** and **Supplementary Movie 2**). Although *Plxna1*$^{-/-}$ DCs actively moved, extended their dendrites and contacted the lymphatic endothelial cells to the same degree as wild-type DCs did, they did not transmigrate across the lymphatic

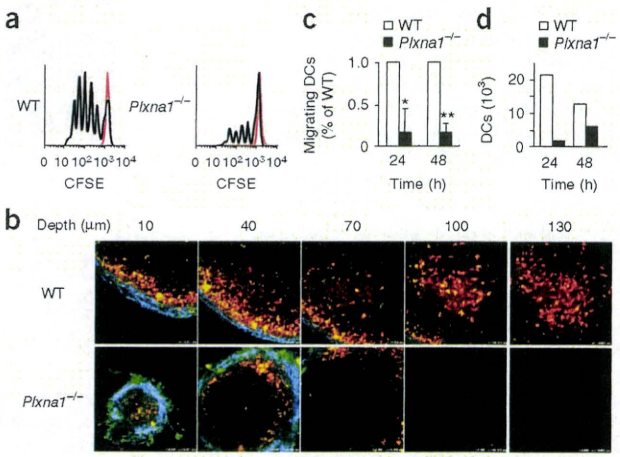

Figure 1 *Plxna1*$^{-/-}$ mice show impaired T cell responses due to defects in the migration of DCs into the lymph nodes. (**a**) CFSE dilution by CD4^{+} OT-II T cells intravenously transferred into wild-type (WT) or *Plxna1*$^{-/-}$ mice given subcutaneous injection of OVA peptides in complete Freund's adjuvant into the footpads, assessed as antigen-specific T cell responses in the draining lymph nodes (black lines) and nondraining lymph nodes (red lines). Data are representative of three independent experiments. (**b**) Two-photon microscopy of CMTMR-labeled wild-type and *Plxna1*$^{-/-}$ bone marrow–derived DCs (BMDCs; orange) injected into the footpads of wild-type recipient mice that also received CMFDA-labeled CD4^{+} OT-II T cells (green), showing DC trafficking into popliteal lymph nodes at 24 h after injection. Original magnification, ×40. Results are representative of two experiments. (**c**) Trafficking of CFSE-labeled wild-type or *Plxna1*$^{-/-}$ DCs into the popliteal lymph nodes of wild-type recipient mice after footpad injection, calculated according to the following equation: (% input cells) = (total cells) × (% CFSE^{+} cells) / (input cells). $^{*}P < 0.01$ and $^{**}P < 0.001$ (Mann-Whitney U-test). Data are representative of three experiments (mean and s.d.). (**d**) Absolute number of endogenous DCs isolated from the brachial lymph nodes of wild-type and *Plxna1*$^{-/-}$ mice at 24 or 48 h after epicutaneous administration of FITC–isomer I to the shoulder skin. Data are representative of three experiments.

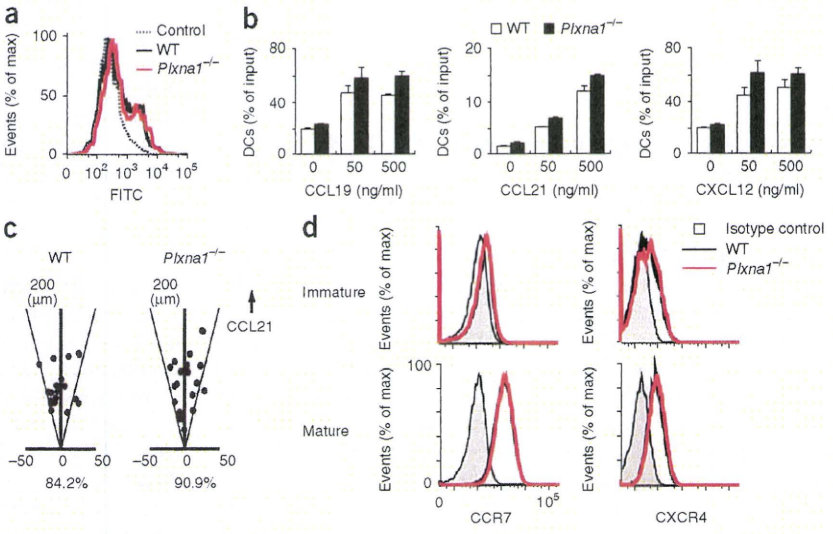

Figure 2 Uptake of FITC-dextran and responses to chemokines are not affected in *Plxna1*$^{-/-}$ DCs. (**a**) Uptake of FITC-dextran by wild-type and *Plxna1*$^{-/-}$ BMDCs at 37 °C for 30 min. Control, cells cultured on ice with FITC-dextran; max, maximum. (**b**) Chemotaxis of wild-type and *Plxna1*$^{-/-}$ DCs toward gradients of CCL19, CCL21 or CXCL12 in Transwell systems (pore size, 5 μm). (**c**) Directional sensing of wild-type and *Plxna1*$^{-/-}$ DCs in response to a CCL21 gradient in a Zigmond chamber, assessed as DC position after 60 min relative to original position and presented as the percentage of cells that ended within a 30° arc facing the CCL21 source. (**d**) Expression of CCR7 and CXCR4 in wild-type and *Plxna1*$^{-/-}$ DCs. Data are representative of three experiments (error bars (**b**), s.d.).

endothelial cells (**Fig. 3b** and **Supplementary Movie 2**), To confirm that observation, we added CFSE-labeled DCs onto monolayers of lymphatic endothelial cells stained with the F-actin marker phalloidin and monitored these cells by confocal *z*-stack imaging. We observed wild-type DCs from the top to the bottom of the endothelial cells. In contrast, although *Plxna1*$^{-/-}$ DCs were able to attach to the lymphatic endothelial cells, they could not transmigrate across these cells (**Fig. 3c** and **Supplementary Movie 3**). Additionally, *Plxna1*$^{-/-}$ DCs showed significantly impaired chemokine-induced transmigration across endothelial cell monolayers in Transwell systems (**Fig. 3d**). Together these results suggest that plexin-A1 has an important role in the transmigration of DCs across the lymphatics.

Sema3A is responsible for plexin-A1-dependent DC trafficking

Plexin-A1 is a receptor component for two types of semaphorins: a secreted class III semaphorin, Sema3A, and class VI transmembrane semaphorins, Sema6C and Sema6D (**Supplementary Fig. 2a**). Notably, Sema3A, Sema6C and Sema6D were all expressed in lymphatic endothelial cells (**Supplementary Fig. 2b**). To determine which interaction was responsible for the defects in *Plxna1*$^{-/-}$ DCs, we adoptively transferred DCs from wild-type mice into *Sema3a*$^{-/-}$ mice[31], *Sema6c*$^{-/-}$ mice (**Supplementary Fig. 4**) and *Sema6d*$^{-/-}$ mice (**Supplementary Fig. 5**). DCs from wild-type mice showed impaired migration to the draining lymph nodes when transferred into *Sema3a*$^{-/-}$ recipient mice (**Fig. 4a**). However, there were no defects in the migration of wild-type DCs in *Sema6c*$^{-/-}$ or *Sema6d*$^{-/-}$ recipient mice (**Fig. 4a**). These results suggest that Sema3A in the lymphatics is indispensable for DC trafficking. Consistent with that, the Sema3A receptor component NRP1 was expressed in DCs (**Supplementary Fig. 2b**). In addition, DCs from *Nrp1*$^{sema-}$ knock-in mice[32], in which the Sema3A-binding sites are defective, showed impaired trafficking to the draining lymph nodes when transferred into wild-type recipient mice (**Fig. 4b**, left). We confirmed those findings by *in vitro* transmigration assays in a lymphatic endothelial cell monolayer and found that DCs from *Nrp1*$^{sema-}$ knock-in mice

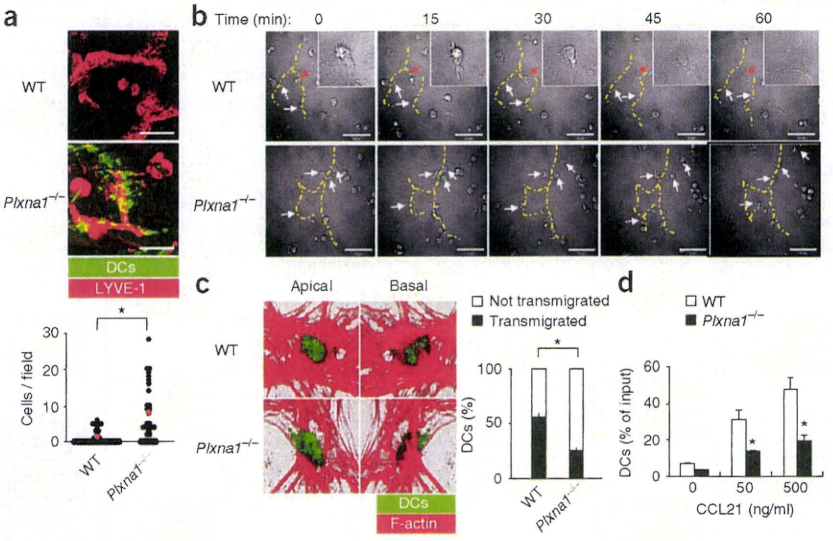

Figure 3 Impaired transmigration of *Plxna1*$^{-/-}$ DCs across the lymphatics. (**a**) Confocal *z*-stack imaging (top) of CFSE-labeled wild-type and *Plxna1*$^{-/-}$ BMDCs (green) injected intradermally into the ear tissues of oxazolone-sensitized mice, assessed in whole mounts stained 24 h after transfer with biotinylated anti–LYVE-1 and streptavidin-indocarbocyanine (red). Scale bars, 50 μm. Below, quantification of retained DCs in the fields above; each symbol represents an individual field, and red circles indicate the mean. *$P < 0.001$ (Mann-Whitney U-test). (**b**) Transmigration of wild-type and *Plxna1*$^{-/-}$ BMDCs across a lymphatic endothelial cell monolayer, assessed by time-lapse video microscopy as interactions recorded every 30 s. Yellow dotted lines indicate junctions of endothelial cells; white arrows indicate DCs in contact with lymphatic endothelial cells; red arrows (top) indicate the transmigration process of wild-type DCs. Scale bars, 50 μm. (**c**) Confocal microscopy (left) of wild-type and *Plxna1*$^{-/-}$ CFSE-labeled DCs added to endothelial cell monolayers, incubated for 45 min, fixed and then stained with Alexa Fluor 546–conjugated phalloidin; images were obtained with an optical section separation (*z*-interval) of 0.22 μm. Right, quantification of DC transmigration, presented as transmigrated DCs relative to total DCs. *$P < 0.001$ (Student's *t*-test). (**d**) Chemotaxis of wild-type or *Plxna1*$^{-/-}$ DC across Transwell inserts (pore size, 5 μm) layered with lymphatic endothelial cell, in response to a CCL21 gradient. *$P < 0.001$ (Student's *t*-test). Data are representative of three experiments (mean and s.d. in **c**,**d**).

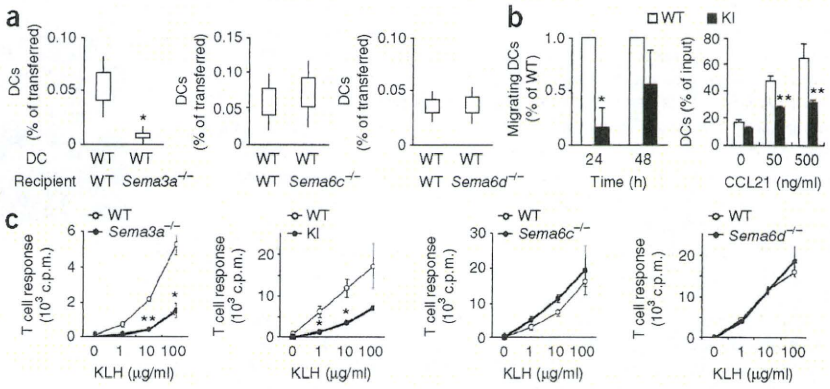

Figure 4 Sema3A–NRP1–plexin-A1 interactions are responsible for DC trafficking. (**a**) Trafficking of wild-type DCs in the lymphatics after adoptive transfer into wild-type, *Sema3a*$^{-/-}$, *Sema6c*$^{-/-}$ or *Sema6d*$^{-/-}$ recipient mice. $^{*}P < 0.01$ (Mann-Whitney U-test). Data are pooled from three independent experiments (standard error ± 95% confidence interval). (**b**) Trafficking of wild-type and *Nrp1*$^{sema-}$ knock-in (KI) DCs into the lymphatics after adoptive transfer into wild-type recipients (left), and chemotaxis of wild-type and *Nrp1*$^{sema-}$ knock-in DCs through Transwell inserts (pore size, 5 μm) layered with lymphatic endothelial cells, in response to a CCL21 gradient (right). $^{*}P < 0.05$ (Mann-Whitney U-test; left) and $^{**}P < 0.01$ (Student's *t*-test; right). Data are representative of three experiments (mean and s.d.). (**c**) *In vitro* proliferation of CD4^{+} T cells in response to keyhole limpet hemocyanin (KLH) after immunization of wild-type, *Sema3a*$^{-/-}$, *Nrp1*$^{sema-}$ knock-in, *Sema6c*$^{-/-}$ and *Sema6d*$^{-/-}$mice with keyhole limpet hemocyanin in complete Freund's adjuvant. $^{*}P < 0.01$ and $^{**}P < 0.001$ (Student's *t*-test). Data are representative of three experiments (mean ± s.d.).

showed impaired transmigration (**Fig. 4b**, right), similar to that of DCs from *Plxna1*$^{-/-}$ mice (**Fig. 3d**). Although DCs expressed Sema6D (**Supplementary Fig. 2b**), DCs from *Sema6d*$^{-/-}$ mice did not show any defects (data not shown). These results indicate that NRP1 expression in DCs is required for DC trafficking. Consistent with those results, *Sema3a*$^{-/-}$ and *Nrp1*$^{sema-}$ knock-in mice had defects in T cell priming (**Fig. 4c**) similar to those of *Plxna1*$^{-/-}$ mice (**Supplementary Fig. 1a**), whereas neither *Sema6c*$^{-/-}$ nor *Sema6d*$^{-/-}$ mice had any defects in antigen-specific T cell priming (**Fig. 4c**). Collectively these results indicate that Sema3A is a functional ligand for plexin-A1 during the trafficking of DCs into the lymph nodes, but Sema6C and Sema6D are not.

Sema3A acts on the rear side of DCs

Sema3A has been identified as a chemorepellent factor that guides the direction of neurons[12], whereas here we have shown that it promotes DC trafficking. Therefore, we hypothesized that cell polarity generated by chemokines during DC migration is critical for the effects induced by Sema3A. To determine the mechanism by which Sema3A regulates DC migration, we did chemotaxis assays by adding Sema3A to the lower or upper chamber of a Transwell system in the presence or absence of chemokines. In the absence of chemokines, Sema3A did not show an effect on spontaneous DC migration. In contrast, in the presence of chemokines, DC chemotaxis was enhanced in Transwell systems when we added Sema3A to the upper chamber, where Sema3A acted on the rear side of DCs, but not when we added Sema3A to the lower chamber (**Fig. 5a**). In two-dimensional directional migration assays evaluated by the EZ-TAXIScan device, Sema3A increased the motility and speed of DCs when it was applied against a chemokine gradient (**Fig. 5b** and **Supplementary Movie 4**). Consistent with those findings, plexin-A1 localized at the trailing edge but not at the leading edge of migrating DCs, where we readily observed actin polymerization (**Fig. 5c,d** and **Supplementary Movie 5**). These results suggest that the effects of Sema3A depend on the polarity of migrating DCs.

Sema3A induces actomyosin contraction via myosin II activity

Myosin II, which is regulated by phosphorylation of MLC[33] and the Rho kinase ROCK, is involved in DC trafficking[11]. The localization

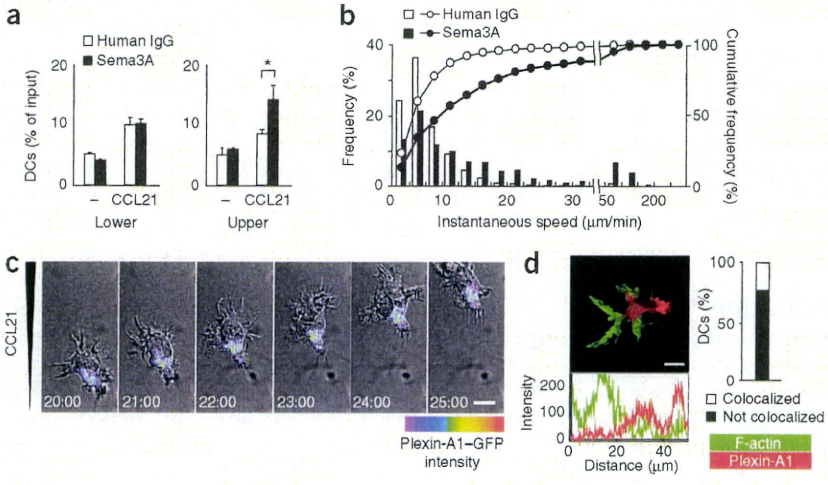

Figure 5 Sema3A acts on the rear side of DCs. (**a**) Chemotaxis of DCs in the presence of human immunoglobulin G (IgG) or recombinant Sema3A protein in the lower (left) or upper (right) chamber of a Transwell system, with CCL21 present (CCL21) or absent (–) in the lower chamber. $^{*}P < 0.01$ (Student's *t*-test). Data are representative of three experiments (mean and s.d.). (**b**) DC speed in a two-dimensional DC chemotaxis assay with Sema3A or human IgG added to the opposite side of CCL21, assessing the frequency distribution (bars) and cumulative frequency distribution (lines) of the instantaneous speed. $P < 0.001$ (Mann-Whitney U-test). Data are representative of three independent experiments. (**c**) Confocal time-lapse video microscopy of BMDCs expressing green fluorescent protein–labeled plexin-A1 (plexin-A1–GFP), treated with lipopolysaccharide, suspended in type I collagen gels and placed into a Zigmond chamber with chemokine gradients; DC locomotion was examined at 1-minute intervals (time (in minutes:seconds), bottom left corner). Scale bar, 10 μm. Results are representative of three experiments. (**d**) Confocal *z*-stack imaging (left) of the localization and intensity of plexin-A1 (anti–plexin-A1 plus indocarbocyanine-labeled anti–rabbit IgG; red) and F-actin (Alexa Fluor 488–conjugated phalloidin; green) in DCs. Scale bar, 10 μm. Right, frequency of cells with no colocalization of signals. Data are representative of three independent experiments.

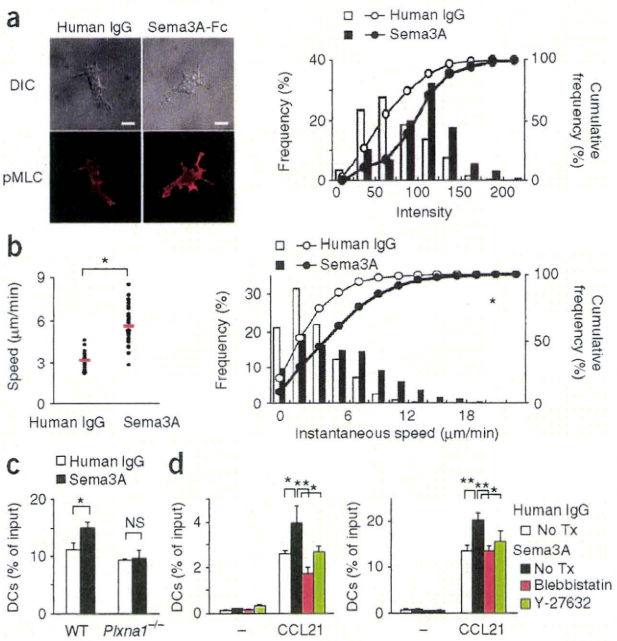

Figure 6 Sema3A induces phosphorylation of MLC and promotes actomyosin contraction. (**a**) Confocal *z*-stack imaging (left) of DCs on fibronectin-coated coverslips treated with human IgG or recombinant Sema3A protein fused with human immunoglobulin Fc portion (Sema3A-Fc) and stained with antibody to phosphorylated MLC (pMLC) plus indocarbocyanine-labeled anti–rabbit IgG (bottom row); eight *z*-stack images with an optical section separation (*z* interval) of 0.36 μm were projected onto one single image. DIC (top row), differential interference contrast image. Scale bars, 10 μm. Right, frequency distribution (bars) and cumulative frequency distribution (lines) of the average intensity of dendrite regions in DCs stimulated with human IgG or Sema3A-Fc. $P < 0.001$ (Mann-Whitney U-test). Data are representative of three independent experiments. (**b**) Speed (left) and frequency distribution (bars, right) or cumulative frequency distribution (lines, right) of the instantaneous speed (right) of a single DC in response to chemokines in the presence of human IgG or Sema3A-Fc in type I collagen matrices, analyzed by time-lapse microscopy and MetaMorph software. Each symbol (left) represents an individual cell; red horizontal lines indicate the mean. $^*P < 0.001$ (Mann-Whitney U-test). Data are representative of three independent experiments. (**c**) Chemotaxis of wild-type or *Plxna1*$^{-/-}$ DCs in response to CCL21 in the presence of human IgG or Sema3A-Fc; DCs were added to the upper chamber of a Transwell system with type I collagen. NS, not significant; $^*P < 0.05$ (overall difference, one-way analysis of variance (ANOVA); post-hoc multiple comparisons, Tukey's test). Data are representative of three experiments (mean and s.d.). (**d**) Chemotaxis of DCs left untreated (No Tx) or treated for 30 min at 37 °C with 50 μM blebbistatin or 30 μM Y-27632 and then added to the upper chamber of a Transwell system (pore size, 5 μm) layered with type I collagen (3 mg/ml; left) and a monolayer of human dermal lymphatic microvascular endothelial cells (right), in response to CCL21 in the presence of human IgG or Sema3A-Fc in the upper chamber. $^*P < 0.05$ and $^{**}P < 0.01$ (overall difference, one-way ANOVA; post-hoc multiple comparisons, Tukey's test). Data are representative of three experiments (mean and s.d.).

of these molecules resembles that of plexin-A1 (ref. 11; **Fig. 5c** and **Supplementary Movie 5**). Myosin II is believed to be required for squeezing of the cell body and induction of actomyosin contraction when cells pass through narrow gaps or constricted areas[11]. In addition, myosin II has been linked to Sema3A-mediated axon retraction[34,35]. Given those findings, we investigated whether Sema3A affects the function of myosin II in DCs during their mobilization. As expected, MLC phosphorylation was enhanced in DCs stimulated with recombinant Sema3A (**Fig. 6a**), and we did not observe this effect in *Plxna1*$^{-/-}$ DCs (**Supplementary Fig. 6**), which indicated that Sema3A promotes MLC phosphorylation via plexin-A1. In three-dimensional collagen matrices, which have been used to model passage through constricted areas *in vitro*, Sema3A increased the speed of DCs and the motile DC fraction (**Fig. 6b** and **Supplementary Movie 6**) and significantly enhanced DC transmigration, and this effect was abolished in *Plxna1*$^{-/-}$ DCs (**Fig. 6c**). In addition, the Sema3A-induced DC transmigration in collagen matrices (**Fig. 6d**, left) or across lymphatic endothelial cell monolayers (**Fig. 6d**, right) was abolished in DCs treated with either the myosin II inhibitor blebbistatin or the ROCK inhibitor Y-27632. Collectively these results suggest that Sema3A induces actomyosin contraction in DCs during plexin-A1-mediated transmigration (**Supplementary Fig. 7**).

DISCUSSION

Although semaphorins were originally identified as axonal guidance cues that regulate cell motility and morphology, accumulating evidence indicates that they also function as immunoregulatory molecules. So far, most functional studies of semaphorins and their receptors have focused on their costimulatory effects on cells of the immune response[17]. Although the nervous and immune systems have considerable crosstalk, and their molecular repertories and machineries overlap[36], it is still unknown whether semaphorins function as guidance cues that physiologically regulate the movement of cells of the immune response. Here we have demonstrated that semaphorin signals are crucial for DC trafficking, particularly for the entry of DCs into the lymphatics. Furthermore, we have highlighted a previously unknown mechanism for DC transmigration across the lymphatics in which Sema3A promotes actomyosin contraction at the trailing edge of migrating DCs so they can pass through narrow gaps.

To exit peripheral tissues, DCs must migrate toward and enter the initial lymphatics. Although it has been assumed that the migration of DCs into the lymphatics is an indolent process, we have provided evidence that Sema3A expressed in lymphatics is crucially involved in DC transmigration. Furthermore, we found that plexin-A1 localized at the trailing edge of migrating DCs, the area responsible for actomyosin contraction. Many factors, including chemokines[6,8], inflammatory molecules[5,37,38] and adhesion molecules[7], have been reported to participate in DC transmigration. However, in our study, neither chemokine responsiveness nor the expression of chemokine receptors was affected in the absence of plexin-A1. The adhesion of DCs to extracellular matrix proteins or to lymphatic endothelial cells was similar in wild-type and *Plxna1*$^{-/-}$ DCs, and the expression of integrins was similar in wild-type and *Plxna1*$^{-/-}$ DCs (data not shown). In addition, there were no differences between wild-type and *Plxna1*$^{-/-}$ DCs in their secretion of the immature form of matrix metalloproteinase 9 and tumor necrosis factor (data not shown). Thus, these results not only indicate that DC transmigration is regulated by active mechanisms but also identify a previously unknown mechanism for this process.

Plexin-A1 is a chief receptor component not only for the soluble semaphorin Sema3A, in association with the receptor NRP1, but also for the transmembrane-type semaphorins Sema6C and Sema6D. We have determined here that Sema3A produced in the lymphatics functioned as a ligand for the plexin-A1–NRP1 receptor complex expressed in DCs, which indicates that the Sema3A–NRP1–plexin-A1 pathways have important roles in DC migration by mediating interactions between DCs and lymphatic endothelial cells. However, it is still unclear why Sema3A, but not Sema6C or Sema6D, is involved in

this process. One possible explanation is that signaling downstream of plexin-A1 is modified by the presence of NRP1 in the receptor. Alternatively, differences in the effects may be due to the fact that Sema3A is a soluble protein. In contrast, Sema6C and Sema6D are membrane-bound semaphorins, which may prevent them from functioning at critical interaction sites between transmigrating DCs and endothelial cells.

Members of the Rho family of small GTPases (Rac1, Cdc42 and RhoA) regulate cell movement by altering actin assembly, adhesion and actomyosin contraction[39]. Among those molecules, Rac1 is required for the generation of actin-rich lamellipodial protrusions and integrin-mediated adhesion[40]. In contrast, RhoA activates ROCK and subsequently activates non-muscle myosin II, which promotes an actomyosin contractile force[41]. Mesenchymal cell movement depends on integrin-mediated traction forces. In contrast, amoeboid cell movement, particularly in three-dimensional environments, does not require integrins. Instead, ROCK- and myosin II–dependent contraction is crucially required for passage through narrow gaps[11]. Consistent with that, we found that Sema3A promoted actomyosin contraction by inducing MLC phosphorylation. Furthermore, this effect was attenuated by blockade of ROCK activity, which indicates that the Sema3A-induced effects on myosin II activity require RhoA-ROCK–mediated signals. In neurons, Sema3A induces the local translation of RhoA in neuronal dendrites[42], and knockdown of RhoA mediated by small interfering RNA blocks Sema3A-mediated collapse of the growth cone[43]. In addition, Sema3A induces MLC phosphorylation, and inhibiting myosin II activity blocks Sema3A-mediated axon retraction[34,35]. These findings indicate that Sema3A-mediated signals promote actomyosin contractile forces through RhoA-dependent activation of myosin II in cells of both the immune and nervous systems.

DCs must pass through various environments. In tissues such as fibroblastic reticular tissues and inner vessel walls, DCs use integrin-mediated attachment and contractile forces for cell movement. In contrast, in constricted areas, DCs use myosin II–mediated actomyosin contractile forces to move forward, because such tissues confine and mechanically anchor cell bodies[44,45]. During DC transmigration, at least three sequential mechanisms may be required. First, DCs must form a lamellipodial protrusion at the leading edge in response to chemokines, which are the driving signal for forward movement. Second, DCs must contract and squeeze their bodies by actomyosin contraction to pass through narrow gaps. Third, after DCs are exposed to the luminal side, the trailing edge must detach from endothelial cells for DCs to enter the circulation. Here we have shown that Sema3A acts on the rear side of DCs through plexin-A1 to promote DC migration. These findings indicate that Sema3A-mediated signals are involved not only in actomyosin contraction but also in the disassembly of adhesive components at the trailing edge during DC transmigration. Indeed, myosin II promotes a traction stress that facilitates detachment at the trailing edge[46,47], which suggests that detachment can be induced by Sema3A-mediated actomyosin contraction. However, Sema3A can inhibit integrin-mediated adhesion by inducing sequestration of the phosphatidylinositol phosphate kinase type I isoform PIPKIγ661 from talin, a chief component of focal adhesion[48]. In this context, it is plausible that Sema3A has dual or integral roles in regulating actomyosin contraction and adhesion disassembly at the trailing edge during the course of DC transmigration.

In conclusion, our study has not only shown the importance of Sema3A-mediated signals in DC trafficking, particularly for passage through the lymphatics, but has also identified a previously unknown mechanism that promotes actomyosin contraction at the trailing edge of migrating cells. As semaphorins are also expressed in vascular endothelial cells[14,16], it is plausible that they have a role in leukocyte extravasation or cancer metastasis. Additional detailed studies are needed to gain insight into these mechanisms, which have the potential to regulate immune reactions for the treatment of autoimmune, allergic and infectious diseases and inhibition of cancer metastasis.

METHODS

Methods and any associated references are available in the online version of the paper at http://www.nature.com/natureimmunology/.

Note: Supplementary information is available on the Nature Immunology website.

ACKNOWLEDGMENTS

We thank D.D. Ginty and A.L. Kolodkin (Howard Hughes Medical Institute) for neuropilin-1-mutant mice; W.R. Heath (University of Melbourne) for OT-II-transgenic mice; and T. Yazawa for technical support. Supported by the Japan Society for the Promotion of Science (Research Fellowships for Young Scientists to H.T.), the US National Institutes of Health (R01NS065048 to Y.Y.), the Ministry of Education, Culture, Sports, Science and Technology of Japan, the Ministry of Health, Labour and Welfare, the Program for Promotion of Fundamental Studies in Health Sciences of the National Institute of Biomedical Innovation (A.K.), the Target Protein Research Program of the Japan Science and Technology Agency (T.T. and A.K.), the Uehara Memorial Foundation (A.K.) and the Takeda Scientific Foundation (T.T., N.T. and A.K.).

AUTHOR CONTRIBUTIONS

A.K. and H.T. designed the study and wrote the manuscript; H.T. did most of the experiments and analyzed the data with Y. Nakagawa, T.O., M.M., S.K. and S.N.; N.T. produced *Sema6d*$^{-/-}$ mice, recombinant Sema6D protein and antibody to Sema6D (anti-Sema6D); M. Tomura did two-photon microscopic experiments; M. Tanaguchi produced *Sema3a*$^{-/-}$ mice; R.H.F., H.R. and M.T.-L. produced *Sema6c*$^{-/-}$ mice; Y.Y. produced anti-plexin-A1; T. Tsujimura did histological analyses; and Y. Nakatsuji, I.K., T. Toyofuku and H.K. provided collaborative suggestions.

COMPETING FINANCIAL INTERESTS

The authors declare no competing financial interests.

Published online at http://www.nature.com/natureimmunology/.
Reprints and permissions information is available online at http://npg.nature.com/reprintsandpermissions/.

1. Steinman, R.M. & Banchereau, J. Taking dendritic cells into medicine. *Nature* **449**, 419–426 (2007).
2. Randolph, G.J., Angeli, V. & Swartz, M.A. Dendritic-cell trafficking to lymph nodes through lymphatic vessels. *Nat. Rev. Immunol.* **5**, 617–628 (2005).
3. Alvarez, D., Vollmann, E.H. & von Andrian, U.H. Mechanisms and consequences of dendritic cell migration. *Immunity* **29**, 325–342 (2008).
4. Forster, R. *et al.* CCR7 coordinates the primary immune response by establishing functional microenvironments in secondary lymphoid organs. *Cell* **99**, 23–33 (1999).
5. Martín-Fontecha, A. *et al.* Regulation of dendritic cell migration to the draining lymph node: impact on T lymphocyte traffic and priming. *J. Exp. Med.* **198**, 615–621 (2003).
6. Ohl, L. *et al.* CCR7 governs skin dendritic cell migration under inflammatory and steady-state conditions. *Immunity* **21**, 279–288 (2004).
7. Johnson, L.A. *et al.* An inflammation-induced mechanism for leukocyte transmigration across lymphatic vessel endothelium. *J. Exp. Med.* **203**, 2763–2777 (2006).
8. Kabashima, K. *et al.* CXCL12-CXCR4 engagement is required for migration of cutaneous dendritic cells. *Am. J. Pathol.* **171**, 1249–1257 (2007).
9. Stoitzner, P., Pfaller, K., Stossel, H. & Romani, N. A close-up view of migrating Langerhans cells in the skin. *J. Invest. Dermatol.* **118**, 117–125 (2002).
10. Baluk, P. *et al.* Functionally specialized junctions between endothelial cells of lymphatic vessels. *J. Exp. Med.* **204**, 2349–2362 (2007).
11. Lammermann, T. *et al.* Rapid leukocyte migration by integrin-independent flowing and squeezing. *Nature* **453**, 51–55 (2008).
12. Kolodkin, A.L., Matthes, D.J. & Goodman, C.S. The semaphorin genes encode a family of transmembrane and secreted growth cone guidance molecules. *Cell* **75**, 1389–1399 (1993).
13. Toyofuku, T. *et al.* Dual roles of Sema6D in cardiac morphogenesis through region-specific association of its receptor, Plexin-A1, with off-track and vascular endothelial growth factor receptor type 2. *Genes Dev.* **18**, 435–447 (2004).
14. Serini, G. *et al.* Class 3 semaphorins control vascular morphogenesis by inhibiting integrin function. *Nature* **424**, 391–397 (2003).

15. Neufeld, G. & Kessler, O. The semaphorins: versatile regulators of tumour progression and tumour angiogenesis. *Nat. Rev. Cancer* **8**, 632–645 (2008).
16. Capparuccia, L. & Tamagnone, L. Semaphorin signaling in cancer cells and in cells of the tumor microenvironment–two sides of a coin. *J. Cell Sci.* **122**, 1723–1736 (2009).
17. Suzuki, K., Kumanogoh, A. & Kikutani, H. Semaphorins and their receptors in immune cell interactions. *Nat. Immunol.* **9**, 17–23 (2008).
18. Kumanogoh, A. *et al.* Identification of CD72 as a lymphocyte receptor for the class IV semaphorin CD100: a novel mechanism for regulating B cell signaling. *Immunity* **13**, 621–631 (2000).
19. Kumanogoh, A. *et al.* Nonredundant roles of Sema4A in the immune system: defective T cell priming and Th1/Th2 regulation in Sema4A-deficient mice. *Immunity* **22**, 305–316 (2005).
20. Takegahara, N. *et al.* Plexin-A1 and its interaction with DAP12 in immune responses and bone homeostasis. *Nat. Cell Biol.* **8**, 615–622 (2006).
21. Suzuki, K. *et al.* Semaphorin 7A initiates T-cell-mediated inflammatory responses through α1β1 integrin. *Nature* **446**, 680–684 (2007).
22. Kruger, R.P., Aurandt, J. & Guan, K.L. Semaphorins command cells to move. *Nat. Rev. Mol. Cell Biol.* **6**, 789–800 (2005).
23. Takahashi, T. *et al.* Plexin-neuropilin-1 complexes form functional semaphorin-3A receptors. *Cell* **99**, 59–69 (1999).
24. Yoshida, Y., Han, B., Mendelsohn, M. & Jessell, T.M. PlexinA1 signaling directs the segregation of proprioceptive sensory axons in the developing spinal cord. *Neuron* **52**, 775–788 (2006).
25. Wong, A.W. *et al.* CIITA-regulated plexin-A1 affects T-cell-dendritic cell interactions. *Nat. Immunol.* **4**, 891–898 (2003).
26. Barnden, M.J., Allison, J., Heath, W.R. & Carbone, F.R. Defective TCR expression in transgenic mice constructed using cDNA-based α- and β-chain genes under the control of heterologous regulatory elements. *Immunol. Cell Biol.* **76**, 34–40 (1998).
27. Mempel, T.R., Henrickson, S.E. & Von Andrian, U.H. T-cell priming by dendritic cells in lymph nodes occurs in three distinct phases. *Nature* **427**, 154–159 (2004).
28. Shortman, K. & Liu, Y.J. Mouse and human dendritic cell subtypes. *Nat. Rev. Immunol.* **2**, 151–161 (2002).
29. Macatonia, S.E., Knight, S.C., Edwards, A.J., Griffiths, S. & Fryer, P. Localization of antigen on lymph node dendritic cells after exposure to the contact sensitizer fluorescein isothiocyanate. Functional and morphological studies. *J. Exp. Med.* **166**, 1654–1667 (1987).
30. Angeli, V. *et al.* B cell-driven lymphangiogenesis in inflamed lymph nodes enhances dendritic cell mobilization. *Immunity* **24**, 203–215 (2006).
31. Taniguchi, M. *et al.* Disruption of semaphorin III/D gene causes severe abnormality in peripheral nerve projection. *Neuron* **19**, 519–530 (1997).
32. Gu, C. *et al.* Neuropilin-1 conveys semaphorin and VEGF signaling during neural and cardiovascular development. *Dev. Cell* **5**, 45–57 (2003).
33. Clark, K., Langeslag, M., Figdor, C.G. & van Leeuwen, F.N. Myosin II and mechanotransduction: a balancing act. *Trends Cell Biol.* **17**, 178–186 (2007).
34. Gallo, G. RhoA-kinase coordinates F-actin organization and myosin II activity during semaphorin-3A-induced axon retraction. *J. Cell Sci.* **119**, 3413–3423 (2006).
35. Brown, J.A., Wysolmerski, R.B. & Bridgman, P.C. Dorsal root ganglion neurons react to semaphorin 3A application through a biphasic response that requires multiple myosin II isoforms. *Mol. Biol. Cell* **20**, 1167–1179 (2009).
36. Boulanger, L.M. Immune proteins in brain development and synaptic plasticity. *Neuron* **64**, 93–109 (2009).
37. Cumberbatch, M. & Kimber, I. Tumour necrosis factor-α is required for accumulation of dendritic cells in draining lymph nodes and for optimal contact sensitization. *Immunology* **84**, 31–35 (1995).
38. Ratzinger, G. *et al.* Matrix metalloproteinases 9 and 2 are necessary for the migration of Langerhans cells and dermal dendritic cells from human and murine skin. *J. Immunol.* **168**, 4361–4371 (2002).
39. Lauffenburger, D.A. & Horwitz, A.F. Cell migration: a physically integrated molecular process. *Cell* **84**, 359–369 (1996).
40. Chhabra, E.S. & Higgs, H.N. The many faces of actin: matching assembly factors with cellular structures. *Nat. Cell Biol.* **9**, 1110–1121 (2007).
41. Vicente-Manzanares, M., Ma, X., Adelstein, R.S. & Horwitz, A.R. Non-muscle myosin II takes centre stage in cell adhesion and migration. *Nat. Rev. Mol. Cell Biol.* **10**, 778–790 (2009).
42. Wu, K.Y. *et al.* Local translation of RhoA regulates growth cone collapse. *Nature* **436**, 1020–1024 (2005).
43. Hengst, U. & Jaffrey, S.R. Function and translational regulation of mRNA in developing axons. *Semin. Cell Dev. Biol.* **18**, 209–215 (2007).
44. Friedl, P. & Weigelin, B. Interstitial leukocyte migration and immune function. *Nat. Immunol.* **9**, 960–969 (2008).
45. Lammermann, T. & Sixt, M. Mechanical modes of 'amoeboid' cell migration. *Curr. Opin. Cell Biol.* **21**, 636–644 (2009).
46. Lombardi, M.L., Knecht, D.A., Dembo, M. & Lee, J. Traction force microscopy in Dictyostelium reveals distinct roles for myosin II motor and actin-crosslinking activity in polarized cell movement. *J. Cell Sci.* **120**, 1624–1634 (2007).
47. Smith, L.A., Aranda-Espinoza, H., Haun, J.B., Dembo, M. & Hammer, D.A. Neutrophil traction stresses are concentrated in the uropod during migration. *Biophys. J.* **92**, L58–L60 (2007).
48. Toyofuku, T. *et al.* FARP2 triggers signals for Sema3A-mediated axonal repulsion. *Nat. Neurosci.* **8**, 1712–1719 (2005).

ONLINE METHODS

Mice. *Plxna1*$^{-/-}$ mice[20] and *Sema3a*$^{-/-}$ mice[31] have been characterized. *Nrp1*$^{sema-}$ knock-in mice were provided by D.D. Ginty and A.L. Kolodkin[32]. OT-II-transgenic mice were provided by W.R. Heath[26]. *Sema6c*$^{-/-}$ and *Sema6d*$^{-/-}$ mice were newly generated as described (**Supplementary Methods**). All experimental procedures were done according to the guidelines of the Research Institute for Microbial Diseases of Osaka University.

Adoptive-transfer experiments. BMDCs were labeled for 10 min at 22 °C with 5 μM CFSE (carboxyfluorescein diacetate succinimidyl ester) in PBS, then were washed extensively with PBS. DCs (1×10^6) in PBS were injected subcutaneously into the hind footpads of recipient mice. Popliteal lymph nodes were collected at 24 and 48 h after injection and then were treated for 30 min at 37 °C with collagenase D (1 mg/ml). Cells were counted and analyzed by flow cytometry. The percentage of migrated DCs corresponds to the ratio of fluorescent DCs among the total lymph node cells[49].

Transwell experiments. Uncoated Transwell inserts (pore size, 5.0 μm; Corning) were placed in 24-well plates filled with 0.6 ml of 0.1% (wt/vol) BSA in RPMI medium containing CCL19, CCL21 or CXCL12. A solution of DCs (1×10^5 cells in 0.1 ml) was added to the upper well of the Transwell, followed by incubation for 3 h at 37 °C. Cells in the lower chamber were detached for 5 min with 5 mM PBS-EDTA and were counted by Guava ViaCount assay on a Guava PCA system. For *in vitro* transmigration assays, fibronectin (10 μg/ml), type I collagen (3.0 mg/ml) or lymphatic endothelial cells were layered on the membrane of the upper chamber. SVEC4-10 mouse lymphoid endothelial cells or human dermal lymphatic microvascular endothelial cells (2×10^4) were seeded on the upper or lower surface of a Transwell insert coated with fibronectin (2 μg/ml). After 2 d of culture, the integrity of the confluent layers was assessed by phalloidin staining. Transmigration assays were done for 6 h as described[50]. Myosin II or ROCK was inhibited by treatment of DCs for 30 min at 37 °C with 50 μM blebbistatin or 30 μM Y-27632, respectively, as described[11].

***In vivo* transmigration of DCs.** For analysis of DCs exiting the periphery, contact hypersensitivity was induced by the application of oxazolone to the abdomen as described[7]. At 6 d after sensitization, oxazolone was applied to the ear; 8 h after challenge, 1×10^6 CFSE-labeled BMDCs were injected dermally. After 24 h, mice were killed and ear tissues were fixed in paraformaldehyde. Whole mounts were stained with biotinylated anti-LYVE-1 (BAF2125; R&D Systems) plus streptavidin-indocarbocyanine for the detection of lymphatics. Images were obtained by confocal *z*-stack imaging and the number of cells retained in the periphery was determined.

Two-dimensional migration assays in three-dimensional collagen matrices. BMDCs that had been treated for 12 h with lipopolysaccharide (500 ng/ml) were suspended in type I collagen (3 mg/ml; BD Biosciences) containing 2% (vol/vol) FCS with either control IgG (5 μg/ml) or Sema3A-Fc (5 μg/ml) and then were placed on one side of the Zigmond chamber to cover the stage with gel. Cells were incubated for 30 min at 37 °C for polymerization of the matrix, and then RPMI medium containing 0.5% (wt/vol) BSA with CCL21 (5 μg/ml) was added to the other chamber. After 20 min of incubation, DC locomotion was examined at 1-minute intervals by confocal time-lapse video microscopy as described above.

Statistical analysis. A two-tailed Student's *t*-test and one-way ANOVA were done after data were confirmed as fulfilling the criteria. Otherwise, the Mann-Whitney U-test and Kruskal-Wallis test were used. If results obtained with the ANOVA or Kruskal-Wallis test were significant, Tukey's test or Scheffe's F-test was used as a post-hoc test. The add-in software Statcel2 was used for analyses.

49. Cavanagh, L.L. *et al.* Activation of bone marrow–resident memory T cells by circulating, antigen-bearing dendritic cells. *Nat. Immunol.* **6**, 1029–1037 (2005).
50. Ledgerwood, L.G. *et al.* The sphingosine 1-phosphate receptor 1 causes tissue retention by inhibiting the entry of peripheral tissue T lymphocytes into afferent lymphatics. *Nat. Immunol.* **9**, 42–53 (2008).

doi:10.1038/ni.1885

Deletion of Sema4D gene reduces intimal neovascularization and plaque growth in apolipoprotein E-deficient mice

KAZUNORI YUKAWA[1], TETSUJI TANAKA[2], MASANORI KISHINO[3], KENJI YOSHIDA[1], NORIKO TAKEUCHI[1], TAKUJI ITO[1], HYOTA TAKAMATSU[4], HITOSHI KIKUTANI[5] and ATSUSHI KUMANOGOH[4]

[1]Department of Physiology, Faculty of Pharmacy, Meijo University, 150 Yagotoyama, Tempaku-ku, Nagoya 468-8503; Departments of [2]Obstetrics and Gynecology; [3]Internal Medicine, Wakayama Medical University, 811-1 Kimiidera, Wakayama 641-8509; Departments of [4]Immunopathology; [5]Molecular Immunology, Research Institute for Microbial Diseases, Osaka University, 3-1 Yamada-oka, Suita, Osaka 565-0871, Japan

Received March 3, 2010; Accepted April 27, 2010

DOI: 10.3892/ijmm_00000432

Abstract. Neovascularization occurring in atherosclerotic plaque leads to acceleration of plaque growth through increased leukocyte infiltration and reactive oxygen species (ROS) production. Sema4D (CD100), a class IV semaphorin, not only plays a crucial role in axon guidance but also functions in the neovascularization process of tumor growth. To clarify the roles of Sema4D in the progression of atherosclerosis and neovascularization of atherosclerotic plaque, we analyzed the effect of Sema4D gene deletion from apolipoprotein E (ApoE)-deficient mice in the development of atherosclerosis. Lipid staining demonstrated significant decreases in plaque areas in the aortas of 6-month-old Sema4D$^{-/-}$ApoE$^{-/-}$ mice compared with 6-month-old ApoE$^{-/-}$ mice. Thus, the Sema4D gene knockout in ApoE-deficient mice was found to slow the progression of atherosclerosis. Immunohistochemical analyses confirmed the expression of Sema4D protein in infiltrating lymphoid cells in atherosclerotic plaque and plexin-B1 receptor in neovascular endothelial cells within the plaque. Furthermore, there were significant decreases in the degree of neovascularization in the plaque areas of Sema4D$^{-/-}$ApoE$^{-/-}$ mice compared with ApoE$^{-/-}$ mice as revealed by both isolectin B4 and CD31 staining. The number of infiltrating macrophages in Sema4D$^{-/-}$ApoE$^{-/-}$ mice plaques was also significantly less than those in ApoE$^{-/-}$ mice. These findings suggest that Sema4D is involved in the progression phase of atherosclerosis by accelerating intimal neovascularization, resulting in enhanced macrophage infiltration in atherosclerotic plaques.

Correspondence to: Dr Kazunori Yukawa, Department of Physiology, Faculty of Pharmacy, Meijo University, 150 Yagotoyama, Tempaku-ku, Nagoya 468-8503, Japan
E-mail: kyukawa@ccmfs.meijo-u.ac.jp

Key words: semaphorin, atherosclerosis, neovascularization

Introduction

Neovascularization not only occurs in the formation stage of highly branched, tree-like tubular networks of blood vessels during development but also in physiological tissue remodeling in adults and the recovery phase subsequent to pathological tissue injury (1). Neovascularization has also been shown to occur in atherosclerotic plaques of human aorta and coronary arteries (1,2). These neovessels originally derive from the adventitial vasa vasorum and nourish thickened atherosclerotic intimal growth (3). Thus, it is a widely accepted hypothesis that neovascularization is one of the major causes of atherosclerotic plaque growth and destabilization (4). Many experiments have suggested the mechanism by which neovascularization promotes atheroma development (5). The strong correlation between the vasa vasorum density and number of mononuclear cells infiltrating the plaque indicates that neovascularization functions as a crucial entry site for leukocyte invasion into atherosclerotic plaque (6,7). Hemorrhaging from plaque neovessels aids blood lipid deposit in the lipid core of atheroma leading to further expansion of the plaque (8). Inhibition of plaque growth through decreased neovascularization in atherosclerosis-prone apolipoprotein E-deficient (ApoE$^{-/-}$) mice with angiogenesis inhibitors such as angiostatin or TNP-470 indicates the functional importance of microvessel growth in the progression of atherogenesis (7,9). Furthermore, neovessels in atheroma are thought to exacerbate atherosclerosis by increasing the intraplaque secretion of metalloproteinase from blood, leading to plaque rupture and thrombus formation (10).

Atherosclerosis is an inflammatory disease in which the immune system plays a major role during disease progression (11). The cell surface molecules CD40 and CD40 ligand (CD40L or CD154) are expressed in macrophages and T cells, respectively (12,13). CD40 ligation involving interaction between CD40 and CD40L on intraplaque cells propagates inflammatory activation by inducing the secretion of proteases and pro-inflammatory mediators (12). Blocking of CD40 ligation and disruption of the gene encoding CD40L respectively reduce atherosclerotic plaques in atherosclerosis-prone mice (14,15). Moreover, stimulation of immune cells with antibodies against CD40 induces the expression of

Sema4D (CD100), a member of the class IV semaphorin family (16). Semaphorins were initially identified as axon guidance molecules playing major roles in the determination of the axonal growth direction during the process of neuronal development (17). Later studies demonstrated various roles of semaphorins in, for example, the immune response, angiogenesis and epithelial morphogenesis (18). Thus, through secretion of soluble Sema4D by proteolytic cleavage of Sema4D extracellular domain from T cell surfaces during mutual immune cell activation mediated by CD40 ligation, Sema4D may exert certain effects on cells residing in atherosclerotic plaques after intraplaque secretion (19-21). Lymphocytes, macrophages, endothelial cells and platelets residing in plaques have a receptor for Sema4D on their membrane surface, namely, plexin-B1 (19-21). Sema4D has pro-angiogenic activity on endothelial cells *in vitro* and *in vivo* (22,23). Even under pathological conditions, high expression levels of Sema4D in several squamous cell carcinomas suggest a critical role in tumor-induced angiogenesis *in vivo* (24). Thus, Sema4D may modulate plaque growth by acting during the neovascularization process occurring in atheroma. By deleting the Sema4D gene in atherosclerosis-prone ApoE$^{-/-}$ mice, we propose that Sema4D promotes intimal neovascularization during plaque growth.

Materials and methods

Mice. Sema4D$^{-/-}$ mice under a C57BL/6J background were generated using the homologous recombination method with ES cells as previously reported (25). ApoE$^{-/-}$ mice (26) in a C57BL/6J background were obtained from The Jackson Laboratory (Bar Harbor, ME). Their progeny were bred to gain mice deficient in both Sema4D and ApoE. After weaning, mice were fed a normal diet. Animals were housed in the animal facilities of Wakayama Medical University and all experimental protocols were approved by the institutional Animal Ethics Review Committee.

Tissue processing. Mice were sacrificed at 6 months of age. The aorta was perfused for 3 min through a 21 gauge needle inserted into the left ventricular apex using phosphate-buffered saline (PBS) and then for another 3 min with 10% phosphate-buffered formalin. The aortic arch with its main branch points (branchiocephalic trunk, left common carotid artery and left subclavian artery) as well as the thoracic and abdominal aorta were excised and fixed in 10% phosphate-buffered formalin. The aorta was then stained with Sudan IV (Sigma-Aldrich, St. Louis, MO) and the percentage of lipid plaque area to total aortic area was quantified using Image J Software (Wayne Rasband, NIH, Bethesda, MD) as previously described (27).

Immunohistochemistry and morphometry. The aortic arch excised from anesthetized mice was fixed in 10% phosphate-buffered formalin. All vessels were embedded longitudinally in paraffin and cut into 4-μm serial sections. Sections were immunolabeled with anti-mouse Sema4D antibody (Medical and Biological Laboratories Co., Ltd. Nagoya, Japan) and anti-mouse CD11b antibody (Serotec, Oxford, UK) to detect macrophages, and anti-mouse CD31 antibody (BD, Franklin Lakes, NJ) to stain endothelial cells. They were subsequently incubated with dextran polymer conjugated with secondary antibodies and peroxidase (DakoCytomation, Kyoto, Japan). To detect neovascularization (28), sections were pretreated with 1 mg/ml protease XIV (Sigma-Aldrich) for 15 min at room temperature and incubated for 1 h at room temperature with 7.5 mg/ml isolectin B4 from *Bandeiraea simplicifolia* conjugated with fluorescein (Sigma-Aldrich). For double immunofluorescence analysis, tissue sections were incubated with anti-mouse CD31 antibody (BD) and anti-plexin-B1 antibody (Santa Cruz Biotechnology, Inc., Santa Cruz, CA). They were then incubated with Alexa-fluor 488 goat anti-rat IgG antibody (Molecular Probes, Eugene, OR) and Alexa-fluor 594 goat anti-rabbit IgG antibody (Molecular Probes) for fluorescent microscopic observation.

The degree of neovascularization was determined as a percentage calculated by dividing the isolectin B4 or CD31-positive area by the respective plaque area using the Image-J morphometry system (Wayne Rasband). The relative area of atherosclerotic plaque positive for infiltrating macrophages was determined by dividing the CD11b-positive area by the total plaque area using Image-J software (Wayne Rasband).

Statistical analysis. Data are expressed as means ±SEM. ApoE$^{-/-}$Sema4D$^{-/-}$ mice were compared with ApoE$^{-/-}$ mice using Student's t-test. Data were considered statistically significant at $p<0.05$.

Results

Delayed development of atherosclerotic plaques in ApoE$^{-/-}$ Sema4D$^{-/-}$ mice. To analyze the effect of Sema4D gene deletion in ApoE-deficient mice on atherosclerosis development, sudanophilic staining of aortas dissected from both ApoE$^{-/-}$ and ApoE$^{-/-}$Sema4D$^{-/-}$ mice was performed. The results revealed a significant delay in atherosclerotic plaque development in aortic regions of 6-month-old ApoE$^{-/-}$Sema4D$^{-/-}$ mice compared with 6-month-old ApoE$^{-/-}$ mice (Fig. 1A). As shown in Fig. 1B, quantitative measurement of atherosclerotic plaque areas demonstrated that the mean percentage of sudanophilic areas to the whole aortic region in 6-month-old ApoE$^{-/-}$Sema4D$^{-/-}$ mice was significantly smaller than that in 6-month-old ApoE$^{-/-}$ mice (ApoE$^{-/-}$Sema4D$^{-/-}$mice, 15.70±2.29% vs. ApoE$^{-/-}$ mice, 23.72±2.57%; $P<0.05$, n=5 for each group).

Sema4D expressed in infiltrating lymphoid cells and plexin-B1 in endothelial cells. Immunohistochemistry to confirm the expression of Sema4D in atherosclerotic plaque showed the localization of Sema4D protein in infiltrating lymphoid cells as shown in Fig. 1C-a. To determine the expression pattern of plexin-B1, a receptor of Sema4D in atherosclerotic plaque, double immunofluorescence studies against CD31, an endothelial marker, and plexin-B1 were performed on plaque areas of atherosclerotic regions. The results demonstrated an overlapping pattern of CD31 (green) and plexin-B1 (red) in plaque areas (Fig. 1C-c and d), indicating plexin-B1 expression on endothelial cells of new vessels growing in the plaques.

Less neovascularization in ApoE$^{-/-}$Sema4D$^{-/-}$ plaques. To study new vessel formation in the atherosclerotic plaques, isolectin B4 staining to detect neovascularization was initially employed

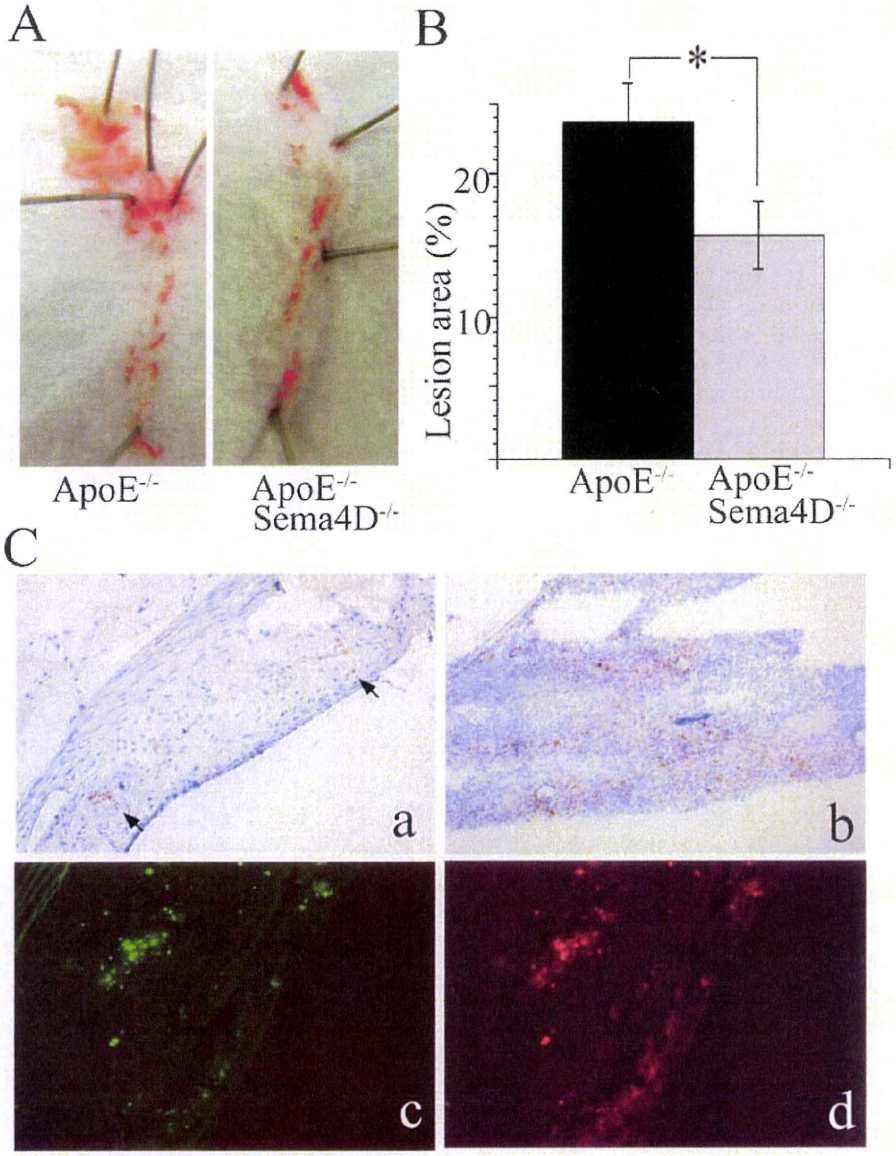

Figure 1. Delayed development of atherosclerotic plaques in ApoE$^{-/-}$Sema4D$^{-/-}$ mice. (A) Sudanophilic staining of aorta disclosed a significant delay in atherosclerotic plaque development in 6-month-old ApoE$^{-/-}$Sema4D$^{-/-}$ mice. (B) The sudanophilic area was significantly smaller in 6-month-old ApoE$^{-/-}$Sema4D$^{-/-}$ atherosclerotic plaques compared with 6-month-old ApoE$^{-/-}$ plaques (n=5 for each group, *p<0.05). (C) Antibodies against Sema4D which bound to lymphocytes in mouse spleen (brown in b) stained infiltrating lymphoid cells in atherosclerotic plaque (brown; arrows in a). Double immunofluorescence analyses revealed that CD31 staining of endothelial cells (green in c) precisely overlapped with the localization of plexin-B1 (red in d), indicating plexin-B1 expression in endothelial cells in atherosclerotic plaques.

with both 6-month-old ApoE$^{-/-}$ and 6-month-old ApoE$^{-/-}$ Sema4D$^{-/-}$ plaques. The results revealed that the percentage of isolectin B4 positive staining in the ApoE$^{-/-}$Sema4D$^{-/-}$ plaques was significantly less than in the ApoE$^{-/-}$ plaques (ApoE$^{-/-}$ Sema4D$^{-/-}$ mice, 0.34±0.15% vs. ApoE$^{-/-}$ mice, 3.04±1.03%; P<0.05, n=7 for each group, Fig. 2A and B). Immunohistochemistry using antibodies against CD31 also confirmed that CD31 positive areas were significantly less in 6-month-old ApoE$^{-/-}$Sema4D$^{-/-}$ plaques compared with 6-month-old ApoE$^{-/-}$ plaques (ApoE$^{-/-}$Sema4D$^{-/-}$ mice, 0.49±0.14% vs. ApoE$^{-/-}$ mice, 3.96±0.81%; P<0.05, n=7 for each group, Fig. 2C and D), underscoring poor neovascularization in Sema4D-deficient plaques.

Less macrophage infiltration in ApoE$^{-/-}$Sema4D$^{-/-}$ plaques. Macrophage infiltration in the atherosclerotic plaques may originate from monocytes circulating in neovessels formed in the plaques (6,7). To examine whether there was less macrophage infiltration in ApoE$^{-/-}$Sema4D$^{-/-}$ plaques, immunohistochemistry with F4/80 antibodies against macrophages was performed on plaques of 6-month-old ApoE$^{-/-}$ and 6-month-old ApoE$^{-/-}$Sema4D$^{-/-}$ mice. As a result, the degree of macrophage infiltration was shown to be significantly lower in 6-month-old ApoE$^{-/-}$Sema4D$^{-/-}$ plaques compared with 6-month-old ApoE$^{-/-}$ plaques (ApoE$^{-/-}$Sema4D$^{-/-}$ mice, 3.90±0.97% vs. ApoE$^{-/-}$ mice, 11.58±2.78%; P<0.05, n= 7 for each group, Fig. 3A and B).

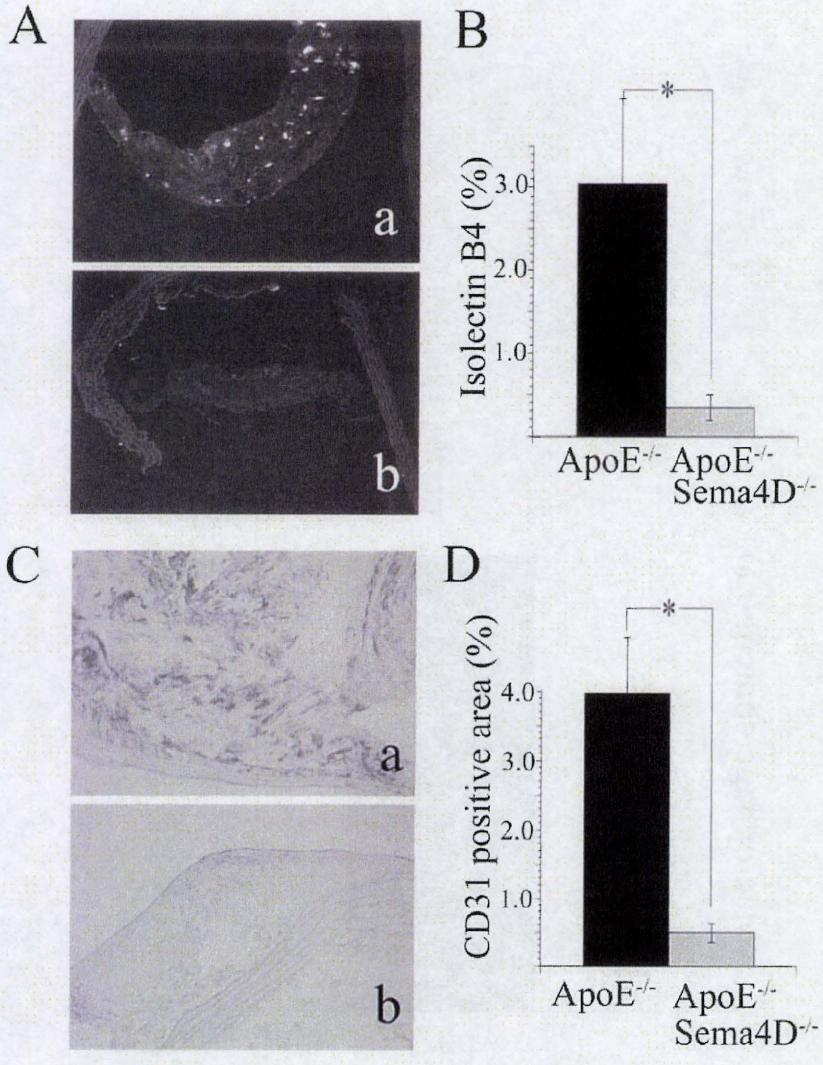

Figure 2. Reduced neovascularization in ApoE$^{-/-}$Sema4D$^{-/-}$ plaques. (A) Neovascularization visualized by isolectin B4 staining in ApoE$^{-/-}$Sema4D$^{-/-}$ plaques (b) appeared to be less than that in ApoE$^{-/-}$ plaques (a). (B) Statistical analyses revealed that the isolectin B4 positive area in 6-month-old ApoE$^{-/-}$Sema4D$^{-/-}$ plaques was significantly smaller than that in 6-month-old ApoE$^{-/-}$ plaques, indicating poor neovascularization in Sema4D-deficient plaques (n=7 for each group, $^{*}p<0.05$). (C) Endothelial cells visualized with immunohistochemistry using CD31 antibodies appeared to be less in 6-month-old ApoE$^{-/-}$Sema4D$^{-/-}$ plaques (b) compared with 6-month-old ApoE$^{-/-}$ plaques (a). (D) Statistical analyses showed that CD31 positive areas were significantly less in 6-month-old ApoE$^{-/-}$ Sema4D$^{-/-}$ plaques compared with 6-month-old ApoE$^{-/-}$plaques, indicating poor microvessels in Sema4D-deficient plaques (n=7 for each group, $^{*}p<0.05$).

Discussion

Our study revealed that deletion of the Sema4D gene in ApoE$^{-/-}$ mice induced significant retardation in atheroma growth, reduction in intimal neovascularization and a decrease in macrophage infiltration in the plaques. Accordingly, our data suggest that Sema4D, secreted into atheroma plaques from the T cell surface as a result of proteolytic cleavage, facilitates plaque growth by promoting neovascularization through induction of endothelial cell migration.

Our finding that deletion of the Sema4D gene from ApoE$^{-/-}$ mice led to significant retardation in plaque growth is comparable with the phenotype of atherosclerosis-prone LDL receptor (LDLR) knockout mice in which the Sema4D gene was also deleted (29). Although in this previous study, the mice were maintained using a high fat diet different from the normal diet employed here, both studies obtained consistent data supporting the promotion of atherosclerosis development by Sema4D. It was proposed that deletion of the Sema4D gene from LDLR$^{-/-}$ mice lessens platelet function leading to retarded atheroma growth (29). Alhough knockout of another platelet related molecule, $\alpha_{IIb}\beta_3$, results in a stronger platelet inhibitory effect than Sema4D knockout, the inhibitory effects of deletion of both genes on atherosclerosis are the same (29,30). This indicates that Sema4D affects the function of other cellular factors in addition to platelets.

Many experiments have supported the concept that intimal neovascularization promotes the growth of atheroma plaque (5,7,9). Factors such as VEGF, IL-8 and Cox-2 play crucial roles in facilitating intimal neovascularization (31-34). Sema4D

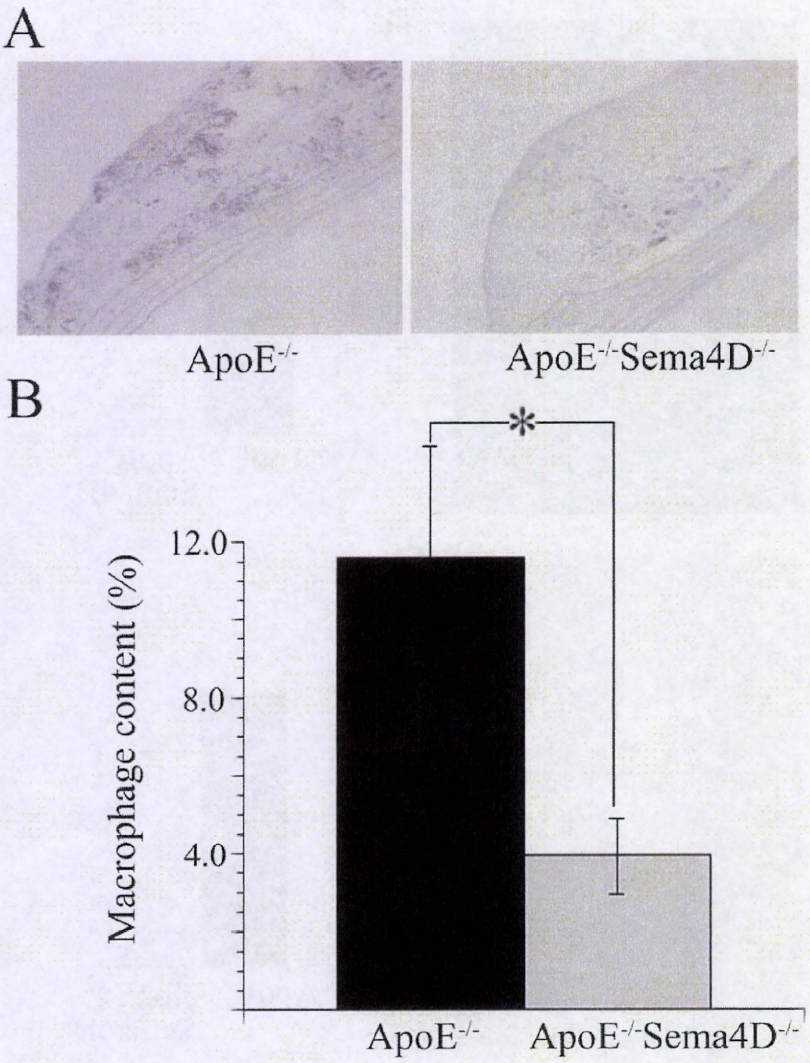

Figure 3. Poor macrophage infiltration in Sema4D-deficient plaques. (A) Macrophage infiltration revealed by immunohistochemistry with F4/80 antibodies appeared to be less in 6-month-old ApoE$^{-/-}$Sema4D$^{-/-}$ plaques than 6-month-old ApoE$^{-/-}$ plaques. (B) Statistical analyses disclosed that the macrophage content in 6-month-old ApoE$^{-/-}$Sema4D$^{-/-}$ plaques was significantly less than in 6-month-old ApoE$^{-/-}$ plaques (n=7 for each group, $^{*}p<0.05$).

displays proangiogenic activity comparable with VEGF and FGF in both *in vitro* and *in vivo* assays (22,23). However, the proangiogenic activity of Sema4D is not thought to be mediated by the up-regulation of VEGF or angiopoietins (22). Determining the specific action exerted by Sema4D in intimal neovascularization, during which factors such as VEGF display major effects, is therefore important. A study of tumor-induced angiogenesis showed that Sema4D works as a directional cue for endothelial cell migration, thus leading to regional neovascularization rather than endothelial cell growth promotion exerted by cytokines such as VEGF (24). It is also known that neovascularization shows regional preference, occurring in atherosclerotic plaque (7,35). Thus, distinct from VEGF, Sema4D may control regional neovascularization by guiding endothelial cell migration into atheroma. Sema4D exerts proangiogenic activity by binding the plexin-B1 receptor expressed on the endothelial cell surface (22,23). Sema4D ligation to plexin-B1 in endothelial cells is integrated not with the rho-rho kinase pathway but with Met receptor-mediated signal transduction machinery (22,23). Interestingly, R-Ras, the activity of which is down-regulated during signal transduction of Sem4D ligation to plexin-B1, also functions to inhibit intimal hyperplasia and tumor angiogenesis (36). This indicates that after binding to plexin-B1 on endothelial cells Sema4D induces intimal growth and angiogenesis by down-regulating R-Ras activity, supporting the present findings. Thus, we propose that Sema4D cleaved and shed from T lymphocytes infiltrating developing atherosclerotic plaque contributes to further atheroma growth by inducing regional neovessel formation as a cue for endothelial cell migration into the plaques. This then results in an increase in macrophage invasion into the plaque from newly produced vessels.

Acknowledgements

We are grateful to K. Kubota, M. Ichinose, T. Ueyama, S. Yukawa and E. Yukawa for their encouragement and support. This study was partly supported by Grants-in-Aid for

Scientific Research from the Ministry of Education, Science, Sports and Culture, Japan.

References

1. Carmeliet P: Angiogenesis in health and disease. Nature Med 9: 653-660, 2003.
2. Zhang Y, Cliff WJ, Schoefl GI and Higgins G: Immunohistochemical study of intimal microvessels in coronary atherosclerosis. Am J Pathol 143: 164-172, 1993.
3. Kumamoto M, Nakashima Y and Sueishi K: Intimal neovascularization in human coronary atherosclerosis: Its origin and pathophysiological significance. Hum Pathol 26: 450-456, 1995.
4. Barger AC, Beeuwkes R 3rd, Lainey LL and Silverman KJ: Hypothesis: vasa vasorum and neovascularization of human coronary arteries. A possible role in the pathophysiology of atherosclerosis. N Engl J Med 310: 175-177, 1984.
5. Moreno PR, Purushothaman KR, Sirol M, Levy AP and Fuster V: Neovascularization in human atherosclerosis. Circulation 113: 2245-2252, 2006.
6. O'Brien ER, Garvin MR, Dev R, Stewart DK, Hinohara T, Simpson JB and Schwartz SM: Angiogenesis in human coronary atherosclerosis plaques. Am J Pathol 145: 883-894, 1994.
7. Moulton KS, Vakili K, Zurakowski D, Soliman M, Butterfield C, Sylvin E, Lo K-M, Gillies S, Javaherian K and Folkman J: Inhibition of plaque neovascularization reduces macrophage accumulation and progression of advanced atherosclerosis. Proc Natl Acad Sci USA 100: 4736-4741, 2003.
8. Kolodgie FD, Gold HK, Burke AP, Fowler DR, Kruth HS, Weber DK, Farb A, Guerrero LJ, Hayase M, Kutys R, Narula J, Finn AV and Virmani R: Intraplaque hemorrhage and progression of coronary atheroma. N Engl J Med 349: 2316-2325, 2003.
9. Moulton KS, Heller E, Konerding MA, Flynn E, Palinski W and Folkman J: Angiogenesis inhibitors endostatin or TNP-470 reduce intimal neovascularization and plaque growth in apolipoprotein E-deficient mice. Circulation 99: 1726-1732, 1999.
10. Jonsson-Rylander AC, Nilsson T, Fritsche-Danielson R, Hammarstrom A, Behrendt M, Andersson JO, Lindgren K, Andersson AK, Wallbrandt P, Rosengren B, Brodin P, Thelin A, Westin A, Hurt-Camejo E and Lee-Sogaard CH: Role of ADAMTS-1 in atherosclerosis: remodeling of carotid artery, immunohistochemistry, and proteolysis of versican. Arterioscler Thromb Vasc Biol 25: 180-185, 2005.
11. Hansson GK and Libby P: The immune response in atherosclerosis: a double-edged sword. Nat Rev Immunol 6: 508-519, 2006.
12. Mach F, Schönbeck U, Bonnefoy JY, Pober JS and Libby P: Activation of monocyte/macrophage functions related to acute atheroma complication by ligation of CD40. Induction of collagenase, stromelysin, and tissue factor. Circulation 96: 396-399, 1997.
13. Mach F, Schönbeck U, Sukhova GK, Bourcier T, Bonnefoy JY, Pober JS and Libby P: Functional CD40 ligand is expressed on human vascular endothelial cells, smooth muscle cells, and macrophages: implications for CD40-CD40 ligand signaling in atherosclerosis. Proc Natl Acad Sci USA 94: 1931-1936, 1997.
14. Mach F, Schönbeck U, Sukhova GK, Atkinson E and Libby P: Reduction of atherosclerosis in mice by inhibition of CD40 signaling. Nature 394: 200-203, 1998.
15. Lutgens E, Gorelik L, Daemen MJ, deMuinck ED, Grewal IS, Koteliansky VE and Flavell RA: Requirement for CD154 in the progression of atherosclerosis. Nat Med 11: 1313-1316, 1999.
16. Kumanogoh A, Watanabe C, Lee I, Wang X, Shi W, Araki H, Hirata H, Iwahori K, Uchida J, Yasui T, Matsumoto M, Yoshida K, Yakura H, Pan C, Parnes JR and Kikutani H: Identification of CD72 as a lymphocyte receptor for the class IV semaphorin CD100: a novel mechanism for regulating B cell signaling. Immunity 13: 621-631, 2000.
17. Raper JA: Semaphorins and their receptors in vertebrates and invertebrates. Curr Opin Neurobiol 10: 88-94, 2000.
18. Kruger RP, Aurandt J and Guan KL: Semaphorins command cells to move. Nat Rev Mol Cell Biol 6: 789-800, 2005.
19. Basile JR, Afkhami T and Gutkind JS: Semaphorin 4D/Plexin-B1 induces endothelial cell migration through the activation of PYK2, src, and the phosphatidylinositol 3-kinase-Akt pathway. Mol Cell Biol 25: 6889-6898, 2005.
20. Delaire S, Billard C, Tordjman R, Chedotal A, Elhabazi A, Bensussan A and Boumsell L: Biological activity of soluble CD100. II. Soluble CD100, similarly to H-SemaIII, inhibits immune cell migration. J Immunol 166: 4348-4354, 2001.
21. Chabbert-de Ponnat I, Marie-Cardine A, Pasterkamp RJ, Schiavon V, Tamagnone L, Thomasset N, Bensussan A and Boumsell L: Soluble CD100 functions on human monocytes and immature dendritic cells require plexin C1 and plexin B1, respectively. Int Immunol 17: 439-447, 2005.
22. Conrotto P, Valdembri D, Corso S, Serini G, Tamagnone L, Comoglio PM, Bussolino F and Giordano S: Sema4D induces angiogenesis through Met requirement by plexin B1. Blood 105: 4321-4329, 2005.
23. Basil JR, Barac A, Zhu T, Guan KL and Gutkind JS: Class IV semaphorins promote angiogenesis by stimulating Rho-initiated pathways through plexin-B. Cancer Res 64: 5212-5224, 2004.
24. Basile JR, Castilho RM, Williams VP and Gutkind JS: Semaphorin 4D provides a link between axon guidance process and tumor-induced angiogenesis. Proc Natl Acad Sci USA 103: 9017-9022, 2006.
25. Shi W, Kumanogoh A, Watanabe C, Uchida J, Wang X, Yasui T, Yukawa K, Ikawa M, Okabe M, Parnes JR, Yoshida K and Kikutani H: The class IV semaphorin CD100 plays nonredundant roles in the immune system: defective B and T cells activation in CD100-deficient mice. Immunity 13: 633-642, 2000.
26. Piedrahita JA, Zhang SH, Hagaman JR, Oliver PM and Maeda N: Generation of mice carrying a mutant apolipoprotein E gene inactivated by gene targeting in embryonic stem cells. Proc Natl Acad Sci USA 89: 4471-4475, 1992.
27. Dougherty A and Whitman SC: Quantification of atherosclerosis in mice. In: Methods in Molecular Biology, vol. 209: Transgenic Mouse Methods and Protocols. Hofker MH and van Deursen J (eds). Humana Press Inc., Totowa, pp293-309, 2002.
28. Lim KY, Ryan EA, Wong PKY and Yuen P-H: Studies on the pathology, especially brain hemorrhage and angioendotheliomas, induced by two new mos-containing viruses. J NeuroVirol 6: 106-120, 2000.
29. Zhu L, Stalker TJ, Fong KP, Jiang H, Tran A, Crichton I, Lee EK, Neeves KB, Maloney SF, Kikutani H, Kumanogoh A, Pure E, Diamond SL and Brass LF: Disruption of Sema4D ameliorates platelet hypersensitivity in dyslipidemia and confers protection against the development of atherosclerosis. Arterioscler Thromb Vasc Biol 29: 1039-1045, 2009.
30. Massberg S, Schrzinger K, Lorenz M, Konrad I, Schulz C, Plesnila N, Kennerknecht E, Rudelius M, Sauer S, Braun S, Kremmer E, Emambokus NR, Frampton J and Gawaz M: Platelet adhesion via glycoprotein IIb integrin is critical for atheroprogression and focal cerebral ischemia: an in vivo study in mice lacking glycoprotein IIb. Circulation 112: 1180-1188, 2005.
31. Celletti FL, Waugh JM, Amabile PG, Brendolan A, Hilficker PR and Dake MD: Vascular endothelial growth factor enhances atherosclerotic plaque progression. Nat Med 7: 425-429, 2001.
32. Schönbeck U, Sukhova GK, Graber P, Coulter S and Libby P: Augmented expression of cyclooxygenase-2 in human atherosclerotic lesions. Am J Pathol 155: 1281-1291, 1999.
33. Simonini A, Moscucci M, Muller DW, Bates ER, Pagani FD, Burdick MD and Strieter RM: IL-8 is an angiogenic factor in human coronary atherectomy tissue. Circulation 101: 1519-1526, 2000.
34. Bochkov VN, Philippova M, Oskolkova O, Kadl A, Furnkranz A, Karabeg E, Afonyushkin T, Gruber F, Breuss J, Minchenko A, Mechtcheriakova D, Hohensinner P, Rychli K, Wojta J, Resink T, Erne P, Binder BR and Leitinger N: Oxidized phospholipids stimulate angiogenesis via autocrine mechanisms, implicating a novel role for lipid oxidation in the evolution of atherosclerotic lesions. Circ Res 99: 900-908, 2006.
35. Moulton KS: Plaque angiogenesis and atherosclerosis. Curr Atheroscler Rep 3: 225-233, 2001.
36. Komatsu M and Ruoslahti E: R-Ras is a global regulator of vascular regeneration that suppresses intimal hyperplasia and tumor angiogenesis. Nat Med 11: 1346-1350, 2005.

Pflugers Arch - Eur J Physiol (2010) 460:875–889
DOI 10.1007/s00424-010-0870-9

NEUROSCIENCE

$GABA_A$ receptor-mediated modulation of neuronal activity propagation upon tetanic stimulation in rat hippocampal slices

Takashi Tominaga · Yoko Tominaga

Received: 14 May 2010 / Revised: 29 July 2010 / Accepted: 9 August 2010 / Published online: 24 August 2010

Abstract Tetanic stimulation (100 Hz), which can induce long-term potentiation in synaptic connections in the hippocampal CA1 region, causes γ-aminobutyric acid $(GABA)_A$ receptor-mediated long-lasting depolarization of postsynaptic neurons. However, it is not clear how this stimulation modulates neuronal activity propagation. We studied tetanic burst-induced neuronal responses in the hippocampal CA1 region by using optical-recording methods employing a voltage-sensitive dye and focused on $GABA_A$ receptor-mediated modulation. We observed that burst stimulation induced long-lasting depolarization and progressive decrease in individual excitatory postsynaptic potentials (EPSPs). Both these effects were suppressed by picrotoxin, a $GABA_A$ receptor antagonist. Under whole-cell voltage-clamp conditions, we observed a long-lasting inhibitory current (IPSC) and a prominent progressive decrease in the amplitude of the excitatory postsynaptic current (EPSC). Further, picrotoxin inhibited the IPSC and the progressive decrease in EPSC. The optically recorded long-lasting depolarization and progressive decrease of EPSPs were strongly dependent on the distance between the recording electrode and the stimulation site. Optical recordings performed across a wide swatch of CA1 revealed that the decrease in activity propagation was followed by facilitation of propagation after recovery and that this facilitation also depended on $GABA_A$ receptors. Intense activation of $GABA_A$ receptors is a key factor shaping the spatiotemporal patterns of high-frequency stimulation-induced responses in the CA1 region.

Keywords Hippocampal slice · GABA · High-frequency stimulus · Voltage-sensitive dye · Optical imaging

Grant sponsor: MHLW Japan; grant number: HSR Grants H20-Kagaku-009

Electronic supplementary material The online version of this article (doi:10.1007/s00424-010-0870-9) contains supplementary material, which is available to authorized users.

T. Tominaga (✉) · Y. Tominaga
Department of Neurophysiology, Kagawa School of Pharmaceutical Sciences, Tokushima Bunri University,
1314-1 Shido,
Sanuki, Kagawa 769-2193, Japan
e-mail: tominagat@kph.bunri-u.ac.jp

T. Tominaga
Laboratory for Dynamics of Emergent Intelligence,
RIKEN Brain Science Institute (BSI),
2-1 Hirosawa,
Wako, Saitama 351-0198, Japan

Introduction

Tetanic stimulation (e.g., stimulation at 100 Hz) of afferent fibers has long been used for the induction of synaptic long-term potentiation (LTP) in the Schaffer collateral pathway in the hippocampal CA1 region [9]. Tetanic stimulation can synaptically induce long-lasting depolarization [27, 32, 50, 51, 53] owing to the depolarizing inhibitory postsynaptic potential generated by intense activation of the $GABA_A$ receptors located on pyramidal cell dendrites [1, 2, 6]. The GABAergic control of plasticity is attributable to transient control of "ionic plasticity" [8, 33, 61].

Using an optical-recording method, we had previously observed that tetanic stimulation elicited long-lasting depolarization of pyramidal cells—especially in the stratum radiatum (SR)—while reducing compound spike firing in the stratum pyramidale and stratum oriens [55]. We also observed that this response to tetanic stimulation exhibits steep convergence at the stimulation site and considered

this convergence to be a consequence of synaptic activation modulation. The neuronal response to tetanic stimulation is most likely to affect the propagation of neuronal excitation and produces more complex propagation patterns than would be expected from a single stimulus. The modified propagation patterns caused by tetanic stimulation may cause heterogeneous LTP induction [16]. In addition, the modification could share the same mechanism that is responsible for complex neuronal activity caused by coherent high-frequency neuronal oscillations, which are important in terms of information processing [5, 13, 24, 42, 47]. In this study, to determine the modulation of activity propagation during tetanic stimulation, we studied synaptic activity and determined its spatiotemporal patterns by using conventional electrophysiological methods in combination with voltage-sensitive dye (VSD) imaging; see the reviews by [17, 26, 48]. Using VSD imaging, we observed membrane potential events in dendrites without causing any of the disturbances in intracellular ion concentration that are possibly caused by electrode insertion; this precaution is an important factor in determining the GABA response [7]. VSD imaging is now used to study population and/or oscillatory activities in various in vitro preparations [3, 4, 11, 18, 35, 37–40, 60, 63], including whole-brain preparations [15, 20, 36].

In this study, we found that tetanic stimulation induced spatiotemporally nonuniform modifications in activity propagation, specifically progressive decrease in excitation propagation upon tetanic stimulation near the stimulation site and facilitation of propagation upon tetanic stimulation at regions distal from the stimulation site along the Schaffer collateral pathway. The progressive decrease in activity propagation during tetanic stimulation was accompanied by a progressive decrease in excitatory postsynaptic currents (EPSCs) under whole-cell voltage-clamp conditions. The results obtained using a $GABA_A$ receptor channel antagonist suggested that progressive decrease in excitatory activity propagation occurs during tetanic stimulation, whereas facilitation of propagation occurs thereafter. Further, the results suggested that both these effects were mediated by $GABA_A$ receptors. We hypothesize that tetanic stimulation-induced $GABA_A$ receptor-mediated modification of neuronal activity propagation is caused by the same mechanism that underlies high-frequency oscillations in the brain.

Materials and methods

Slice preparation and staining with VSD

All animal experiments were performed according to protocols approved by the Animal Care and Use Committee of Tokushima Bunri University. Hippocampal slices (400 μm thick) were prepared from 4- to 5-week-old male rats, decapitated under deep ether or isoflurane anesthesia. The brains were quickly removed and cooled in ice-cold artificial cerebrospinal fluid (aCSF; 124 mM NaCl, 2.5 mM KCl, 2 mM $CaCl_2$, 2 mM $MgSO_4$, 1.25 mM NaH_2PO_4, 26 mM $NaHCO_3$, and 10 mM glucose, pH 7.4) bubbled with 95:5% O_2/CO_2 gas. After cooling for 5 min, the hippocampus was dissected out along with the surrounding cortex and sliced into 400-μm-thick transverse sections with a vibratome (Leica VT-1000). A cut was made through the slices at the CA3/CA1 border to prevent seizure propagation from the CA3 region. Following incubation in gassed aCSF for 3–5 min, each slice was transferred onto a fine-mesh membrane filter (Omni Pore membrane filter, JHWP01300; Millipore Corp., Billerica, MA, USA), held in place by a thin Plexiglas ring (inner diameter, 11 mm; outer diameter, 15 mm; thickness, 1–2 mm). These slices were transferred to a moist chamber continuously supplied with a humidified O_2/CO_2 gas mixture. The temperature was held at 32°C for 1 h and then maintained at room temperature thereafter. After 1 h incubation, each slice was stained for 25 min with 100 μl of the VSD solution, containing 0.2 mM di-4-ANEPPS (Molecular Probes) in 2.5% ethanol, 0.13% Cremaphor EL (Sigma), 1.17% distilled water, 48.1% fetal bovine serum (Sigma), and 48.1% ACSF. The slices were subjected to experiments after at least a 1-h incubation at room temperature after the washout of VSD.

Optical recording

The Plexiglas ring supporting each slice was placed in an immersion-type recording chamber. Slices were continuously perfused with prewarmed (31°C) and oxygenated aCSF (bubbled with a 95:5% O_2/CO_2 gas mixture) at a rate of 1 ml/min. Custom laboratory-designed epifluorescence optics consisting of two principal lenses were used to view the slices during experiments. The optics consisted of a modified 35-mm camera lens (f=50 mm F/1.4, Nikon; the final magnification of the system was ×1.5) and another lens (f=55 mm×1.0 Leica Microsystems MZ-APO) as the projection lens. Excitation light was provided by a halogen lamp source (150 W; MHW-G150LR; Moritex Corp.) projected through an excitation filter ($\lambda = 530 \pm 10$ nm) and reflected onto the hippocampal slice by a dichroic mirror (λ=575 nm). Emission fluorescence from the slice was passed through an emission filter (λ>590 nm) and projected onto a CCD camera (MiCAM01; BrainVision, Inc., Tokyo, Japan). The high-speed imaging system provided a spatial resolution of approximately 22×22 μm at the objective plane (96×64 pixels resolution) and a temporal resolution of 0.7 ms/frame.

The intensity of fluorescence emitted by the slice prior to stimulation (a prestimulation period usually lasted from 100 to 740 frames) was averaged and used as a reference intensity (F_0). The fractional change in fluorescence $[\Delta F(t) = F(t) - F_0]$ was normalized by the F_0 ($\Delta F/F_0$), and this value was used as the optical signal. Optical signals referred to in the following sections represent signals filtered in spatial and temporal dimensions with a digital Gaussian kernel of 5×5×3 (horizontal × vertical × temporal; $\sigma \approx 1$). In some experiments, we observed a slow drift of the baseline signal; in these cases, the drift was compensated for by subtracting a normalized smooth spline curve, obtained from optical signals recorded at pixels where no response was observed (e.g., optical signals in the hilus). We confirmed that this procedure produced steady and flat baseline signals and did not cause an artificial drift in the absence of stimulation.

We analyzed optical signals offline using a procedure developed for Igor Pro (WaveMetrics Inc., Portland, OR, USA). At a wavelength of 610 nm, VSD fluorescence decreases in response to the depolarization of the membrane. To fit the polarity of the response to conventional membrane potential changes, we expressed the optical signal in a polarity that matched the membrane potential change. For example, decreased fluorescence, which corresponds to depolarization, was represented as a positive deflection. For additional details on the methods, see [54–57].

We used tetanic stimulation consisted of 40 stimuli at 100 Hz instead of "classical" 100 stimuli to record the signal at higher frame rate within a fixed maximum frame length. The response was not qualitatively different in these protocols.

Electrophysiological recording and stimulation

Patch-clamp recordings in whole-cell mode were made using a patch-clamp amplifier with a capacitive head stage (Axoclamp 700B; Axon Instruments, Foster City, CA, USA). Pipettes of borosilicate glass (Sutter Instruments, Novato, CA, USA) were pulled using a P-97 Flaming–Brown pipette puller (Sutter Instruments, Novato, CA, USA). The K-based pipette internal solution used for current clamp experiments consisted of (in millimolars) 120 K-gluconate, 20 KCl, 10 Hepes, 4 NaCl, 4 Mg_2SO_4, 0.3 NaGTP, and 14 Na_2-phosphocreatine; pH was adjusted to 7.0 (6–7 MΩ). The Cs-based pipette internal solution used for whole-cell voltage-clamp experiments consisted of (in millimolars) 120 Cs-$MeSO_3$, 10 Hepes, 4 $MgCl_2$, 4 NaATP, 0.4 NaGTP, 10 Na-phosphocreatine, 5 QX-314, and 10 EGTA; pH was adjusted to 7.2 (2–4 MΩ). We also used a Cs-based pipette internal solution with higher Cl^- concentration for some whole-cell voltage-clamp experiments, which consisted of (in millimolars) 86 Cs-$MeSO_3$, 34 CsCl, 10 Hepes, 4 $MgCl_2$, 4 NaATP, 0.4 NaGTP, 10 Na-phosphocreatine, 5 QX-314, and 10 EGTA; pH was adjusted to 7.2 (2–4 MΩ).

Whole-cell recordings were low-pass-filtered at 3 kHz and digitized at 10 kHz (ITC-18; Instrutech Inc., Elmont, NY, USA). Data were fed into an Apple computer for online and offline analysis using laboratory-developed software on IgorPro (WaveMetrics Inc., Portland, OR, USA). Electrical stimuli were constant current pulses (A395, WPI) applied through a glass microcapillary pipette (5 μm inner diameter; filled with aCSF). We used oblique illumination to view neurons with a CMOS camera (SKDCE-2EX; Sigma Koki Co., Tokyo, Japan) attached to an upright microscope (BX-51WI; Olympus Tokyo, Japan). In voltage-clamp mode, a test membrane potential step (−10 mV) was always applied prior to electrical stimulation, and traces with series resistance (R_s) lower than 20 MΩ were accepted.

A laboratory-made differential amplifier and a general-purpose amplifier (model 440; Brownlee Precision, San Jose, CA, USA) were used for field potential recordings. Cells with resting membrane potentials between −65 and −80 mV were accepted for study. Glass microcapillary pipettes (5 μm inner diameter; filled with aCSF) were used for both monopolar stimulation and extracellular field potential recordings.

The electrophysiological recording system was controlled by a procedure developed in Igor Pro (WaveMetrics Inc., Portland, OR, USA). High-frequency stimulation of the Schaffer collaterals consisted of bipolar (200 μA, 200 μs width) pulses applied at 100 Hz (40 pulses). Artifacts caused by electrical stimulation were digitally removed from the traces shown in the "Results" section. To monitor synaptic transmission in CA1, in most experiments, we applied a 0.05- to 0.1-Hz stimulus at an intensity that produced an approximately 30% maximal field excitatory postsynaptic potential (fEPSP). The electrophysiological recording and the optical recording did not interfere with each other.

Drugs and solutions

All experiments were done in the presence of 50 μM DL-2-amino-5-phosphonovaleric acid (APV; Tocris). In our previous paper, we established that 50 μM APV had no effect on a burst stimulation-induced response in CA1, even though posttetanic potentiation did affect the amplitude of the response [55]. We took advantage of this lack of an effect in the presence of APV to allow multiple episodes of tetanic stimulation to be applied in a single slice and to improve the signal-to-noise ratio of optical signals by averaging. The optical signals presented in later sections were the average of four episodes. Unless otherwise stated, 50 μM APV was always added to the perfusate. Even in the

presence of APV, at least a 4-min "rest" interval was interposed between separate episodes of high-frequency stimulation to avoid changes in the responses [53]. Picrotoxin (PiTX) was dissolved in ethanol to make a 50-mM stock solution. The low Ca^{2+} aCSF had the following ion concentrations: 124 mM NaCl, 2.5 mM KCl, 0.25 mM $CaCl_2$, 4 mM $MgCl_2$, 2 mM $MgSO_4$, 1.25 mM NaH_2PO_4, 26 mM $NaHCO_3$, and 10 mM glucose, pH 7.4. Other common reagents were obtained through local resellers in Japan.

When there was a significant difference between groups, Tukey's multiple comparison test was performed to determine the levels of significance on IgorPro software. All the measurements are presented as mean±SEM, and n means the number of slices tested unless otherwise stated.

Results

Tetanic stimulation (100 Hz)-induced progressive decrease in EPSPs measured using optical signals

High-frequency (100 Hz) tetanic burst stimulation applied to the middle of the SR of CA1 typically elicited a long-lasting depolarizing optical signal [55] (for a video of these optical recordings under normal conditions, please see Supplemental movie s1.mpg). Optical signals obtained from the SR indicated a tetanus-induced long-lasting depolarizing response on which individual responses, i.e., EPSPs, to individual stimulation pulses were superimposed (black trace in Fig. 1b). On measuring the height of each peak amplitude from the bottom of the inter-EPSP response, we observed that the amplitude of individual EPSPs appeared to decrease.

For a more detailed study of the progressive decrease, we attempted to separate the individual EPSPs from the long-lasting depolarizing component. A profile drawn tangent to the wave troughs between individual responses should provide a fair representation of the time course of the long-lasting depolarization. Hence, we chose the minimum peak between each response as the representative data for the fit of a long-lasting depolarization. We started with the simplest single exponential equation:

$$f(t) = a(1 - \exp(-t/\tau)) \quad (1)$$

where a is the maximum amplitude of the response and τ is the time constant. Since the data points in the first 200 ms appeared to contain a component that would not fit in Eq. 1, we excluded these data points. The resulting fit is shown as a blue line in Fig. 1b. The subtraction of this curve from the data representing the optical signal is shown in Fig. 1c as a black trace (please also see Supplemental movie s2.mpg). The subtracted trace (black trace in Fig. 1c) shows that the amplitudes of individual responses in this residual potential decreased with increasing number of tetanic

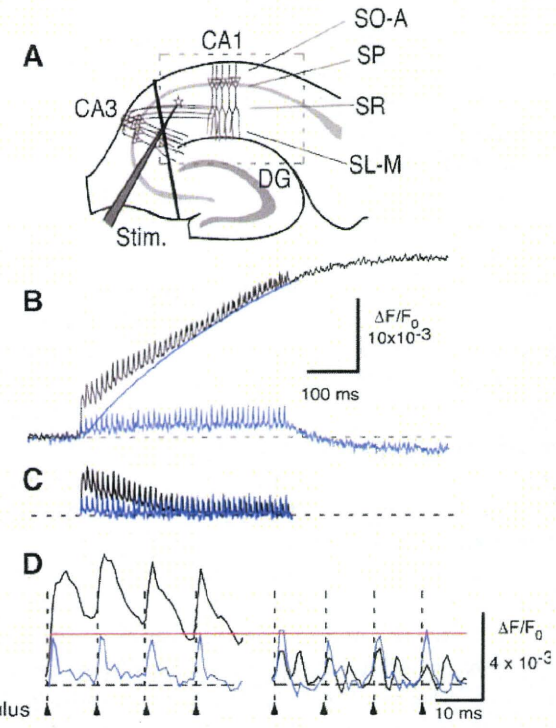

Fig. 1 Progressive decrease in EPSPs during tetanic stimulation. **a** A schematic of hippocampal slice preparation and the field of view of the imaging system (*dashed square*). *SO-A* stratum oriens–alveus, *SP* stratum pyramidale, *SR* stratum radiatum, *SL-M* stratum lacunosum–moleculare. **b** The *black line* is a representative trace of the optical signal obtained at a pixel in the middle of the stratum radiatum in the CA1 region in response to tetanic stimulation (100 Hz, 40 pulses; see also Supplemental movie s1.mpg), and the *blue line* is a trace of the optical signals obtained using aCSF with a low Ca^{2+} content. This aCSF contained 0.25 mM Ca^{2+} and 6 mM Mg^{2+}. The smooth *blue line* represents the curve resulting from single exponential fit of the data (see "Results" section for more details). **c** The residual curve resulting from the subtraction of the smooth blue line from data representing the optical signals shown in **b** is superimposed on the response obtained using the aCSF with a low Ca^{2+} content (*blue trace*). **d** The traces in **c** are displayed together with expanded time and amplitude scales; these have been taken from the initial (*left*) and final phases (*right*) of tetanic stimulation. The timings for stimulation are indicated at the *bottom of the figure* (*arrowheads*). The *red horizontal line* indicates the amplitude of the fast transient response in the low Ca^{2+} content solution; the amplitude of the fast transient did not change during tetanus

stimuli, suggesting that EPSPs incrementally decreased in accordance with tetanic stimulation. The amplitude of the optical signal to the first stimulation was significantly larger than that to the last (40th) stimulation (first stimulation, $4.04 \times 10^{-3} \pm 0.66 \times 10^{-3}$; 40th stimulation, $0.75 \times 10^{-3} \pm 0.09 \times 10^{-3}$; $n=7$; $P<0.001$; the optical signal was measured at 200 μm from the stimulation site). The fitted amplitude of the long-lasting depolarization (a) was the largest near the stimulating electrode and decreased at points located away from the stimulating electrode. The time constant (t) was approximately 480 ms for EPSPs recorded

around the stimulating electrode and decreased to 200 ms at the farthest point from the electrode.

The optical signal consisted of the postsynaptic membrane potential response from a population of pyramidal cells and the population presynaptic fiber activity. We noticed that the small fast components corresponding to each stimulus were superimposed on the long-lasting depolarization and thought that this could be attributable to presynaptic fiber activity. In order to investigate whether presynaptic fiber activity is responsible for the small fast components that crown the long-lasting slower depolarization and correspond to each stimulus, we repeated these experiments after suppressing synaptic transmission by a low Ca^{2+} aCSF. Most of the long-lasting component was absent when the perfusate contained reduced levels of Ca^{2+} (blue trace in Fig. 1b); the amplitude of the residual fast transient responses did not change during tetanus. The fast transient responses were sensitive to tetrodotoxin, except in the close vicinity of the stimulating electrode; therefore, we conclude that these responses can be attributed to presynaptic fiber activity. The responses recorded in aCSF with a low Ca^{2+} content (blue traces) and the subtracted response (black trace) have been compared in Fig. 1c. The traces from the initial (left) and final phases of the tetanus (right) are displayed with expanded time and amplitude scales in Fig. 1d. The amplitude of the fast transient response in aCSF with a low Ca^{2+} content did not change during the tetanus (first stimulation, $1.21 \times 10^{-3} \pm 0.48 \times 10^{-3}$; 40th stimulation, $1.11 \times 10^{-3} \pm 0.36 \times 10^{-3}$; n=3). The amplitude of the fast transient response, which corresponds to presynaptic fiber activity, is indicated by the horizontal red line. The subtracted signal amplitude (black trace) during the initial phase was larger than the fast transient response, whereas the signal amplitude during the last phase showed two peaks for each stimulation (arrowheads under the traces). The latter peak, which should correspond to the EPSP, was smaller than the fast transient response (red line). The fast presynaptic activities of the subtracted trace were similar to those measured in low Ca^{2+} solution after the initiation of fitting, i.e., after 200 ms from the initiation of tetanic stimulation; therefore, we can postulate that the observed decrease in the later individual EPSP components in the subtracted trace may correspond to the progressive decrease in EPSPs.

Progressive decrease of EPSPs and EPSCs during high-frequency tetanic stimulation

To confirm that the progressive decrease is not an artifact of the optical-recording technique, electrophysiological responses corresponding to the same stimulation were also examined (Fig. 2). High-frequency stimulation produced repetitive fEPSPs recorded from the middle of CA1 SR (Fig. 2a). The individual responses were superimposed on a slow negative potential shift lasting about 1 s. The amplitude

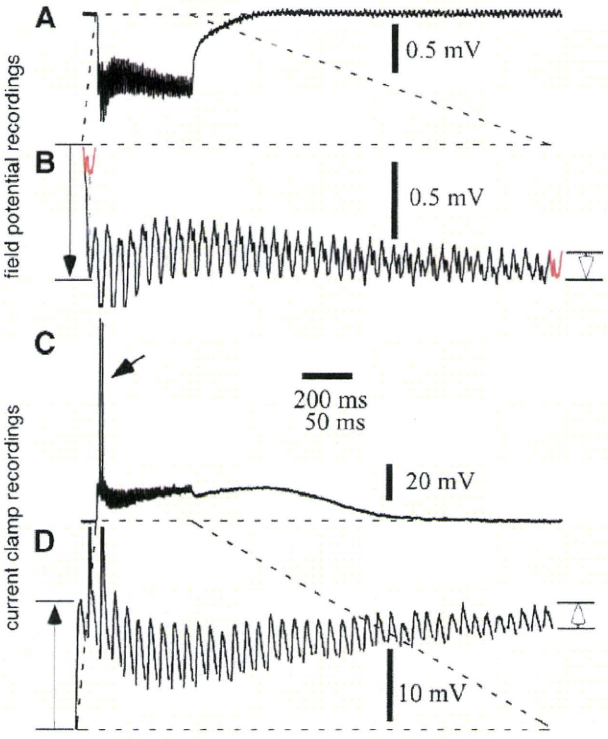

Fig. 2 Progressive decrease of excitatory postsynaptic potentials (EPSPs) in response to tetanic stimulation (100 Hz, 40 pulses) and field potentials (fEPSPs) in rat hippocampal CA1 slices. **a**, **b** Field potential recording. Representative field potential changes in response to the tetanic stimulation; recorded with an extracellular electrode positioned in the middle of stratum radiatum (about 200 μm from stratum pyramidale, 400 μm from stimulating electrode) of the slice. The response to the last stimulus was highlighted in *red color* and was also superimposed in the first response in trace **b**. A *blue dashed line at the first response* shows the timing of the peaks. **c**, **d** Representative trace of membrane potential responses recorded under current clamp. There are two APs at the beginning of the tetanic stimulation (*arrow*). These APs are truncated in **d**. *Bottom ticks* illustrate the timing of the stimulation pulses. Traces were acquired in the presence of 50 μM of APV in the perfusate (see "Materials and methods" section)

of the individual responses seemed to gradually decrease with increase in the number of afferent shocks, as shown in the time-expanded scale (Fig. 2b). That is, the amplitude of the first response (closed arrow) was significantly larger than that of the last response (red colored; open arrow; −1.02± 0.23 mV to the first stimulation, −0.34±0.08 mV to the 40th stimulation, P<0.05, n=5). For comparison, the response to the 40th stimulus was highlighted in red and was also superimposed on the first response in Fig. 2b. It was obvious that the last response consisted of two peaks. This can be interpreted to reflect the fiber volley caused by presynaptic fiber activity and the fEPSP, as was similarly observed in the optical signal in Fig. 1d. That is, fEPSP amplitude progressively decreased, while the presynaptic fiber volleys were preserved. This corresponds to the two peaks observed in the optical signal shown in Fig. 1d.